# Experimental Results of Pitching Moment Tests on Parabolic-Trough Solar-Collector Array Configurations

Duane E. Randall, Roger E. Tate, David A. Powers

SF 2900-Q(6-82)

# Experimental Results of Pitching Moment Tests on Parabolic-Trough Solar-Collector Array Configurations

Duane E. Randall
Solar Systems Applications Division 9727

Roger E. Tate
David A. Powers
Experimental Aerodynamics Division 1634
Sandia National Laboratories
Albuquerque, NM 87185

## Abstract

Two wind-tunnel tests were conducted to investigate specifically the pitching moment characteristics of parabolic-trough solar-collector modules deployed within a collector array. The collector modules were located within various rows of a simulated array configuration to investigate shielding effects from upstream collector rows and/or wind-screen fences. Selected fence configurations and fence spacing upstream from the initial array row were studied. The test results demonstrate that pitching moment is significantly reduced by shielding provided by upstream fencing or collector rows.

# Contents

# Figures

# Experimental Results of Pitching Moment Tests on Parabolic-Trough Solar-Collector Array Configurations

# 1. Introduction

To a large extent, the pitching moment characteristics of the solar-collector module determine the design requirements for the tracking drive system of line-focus collector arrays. The aerodynamic characterization of parabolic-trough solar-collector configurations have been undertaken in two previous wind-tunnel tests. The first of these tests,[1] conducted in a uniform velocity, low turbulence, unbounded airstream, provided basic reference aerodynamic force and moment characteristics for an isolated individual parabolic-trough collector module. The second test,[2] conducted in a simulated atmospheric boundary-layer flow, attempted to investigate the influence of shielding on a collector module embedded at various depths within a ground-mounted array. Limited data were also obtained to evaluate the shielding effects provided by fences or selected berm configurations upwind from the perimeter row of a collector array. The test results indicated that shielding significantly reduced lateral (drag) and lift forces on a collector module; surprisingly, however, this effect did not extend to the pitching moment characteristics. Subsequently, two additional wind-tunnel tests were conducted to verify the pitching moment characteristics of parabolic-trough solar-collector modules. These two tests, together with the experimental data obtained, are described in this report.

# 2. Experimental Conditions and Test Techniques

Previous SNLA aerodynamic test commitments scheduled in the LTV Low Speed Wind Tunnel afforded an opportunity for a rapid entry to conduct 2 days of testing to validate the pitching moment characteristics obtained in Reference 2. However, when these test results contradicted (rather than substantiated) the previous shielded pitching moment data, a more comprehensive pitching moment test program was undertaken in the Meteorological Wind Tunnel at Colorado State University.

## 2.1 TEST I (LTV)

TEST I was conducted in the Low Speed Wind Tunnel of the LTV Corporation, the same facility used for the test program described in Reference 1. This facility, designed for flight vehicle testing, provides a low-turbulence, uniform-velocity airstream with a maximum velocity capability of 238 mph in the 7- by 10-ft test section. This test was conducted at a free-stream dynamic pressure of $\sim$75 lb/ft$^2$, corresponding to a flow velocity of 175 mph. This environment results in a Reynolds number based upon model aperture width of $\sim$1 $\times$ 10$^6$. The typical full-scale Reynolds number at design wind-survival conditions would be 4 to 5 million.

To provide a scaled simulation of a ground-mounted collector array, all the test models were mounted on an aluminum base plate attached to the floor of the wind tunnel. An additional blank plate was installed on the test-section floor upstream from the model station to provide a smooth floor surface extending from the tunnel contraction section to a station downstream from the aft model location. A pretest calibration demonstrated that the flow velocity at collector centerline height above the tunnel floor was equal to the test section centerline velocity. These data indicate that the boundary-layer thickness at the test section floor was less than half the model aperture and suggests that the models did not experience a significant velocity profile across the aperture during this test.

## 2.2 TEST II (CSU)

TEST II was conducted in the Meteorological Wind Tunnel at the Fluid Dynamics and Diffusion Laboratory of Colorado State University, the same facility used for the test program described in Reference 2. This facility simulates the atmospheric boundary layer by using upstream spires and roughness elements on the tunnel floor to generate velocity and turbulence profiles in the tunnel test section. The tunnel was configured to reproduce the test environment used during the Reference 2 test program. The 6 ft 8 in. by 6 ft high test section provided a flow velocity of 52 mph at the edge of the boundary layer (4.1 ft above the test section floor). The boundary-layer velocity profile, determined by hot-wire surveys, approximated a power-law profile with an exponent of 0.152. Turbulence intensity varied from approximately 5% at the edge of the boundary layer to 19% at the floor with 16% at collector centerline height. The boundary-layer velocity and turbulence profile data are illustrated in Figure 1. This environment provides a free-stream dynamic pressure at collector centerline height of 2.3 lb/ft$^2$ and a Reynolds number based on collector aperture width of $\sim$60 000.

As in the previous test, the collector-array model was mounted to the wind-tunnel floor to simulate ground-mounted full-scale installations.

## 2.3 Model Configurations and Instrumentation

At each test facility, the same collector models (fabricated for the original test series)[1,2] were reused for these moment tests by modifying the model-mounting attachment.

### 2.3.1 TEST I (LTV)

For this test, solar-collector models (fabricated for the initial LTV test) were modified to provide three collector modules corresponding to the 3.7 aspect ratio configuration. The original sting-mount arrangement was removed and the parabolic-trough section of the model was attached (through a fairing added to the rear surface) to a 0.75-in.-dia steel shaft spanning the model length. The steel shaft served as the pivot axis, resulting in a pivot-center location 0.0716 aperture widths behind the vertex of the parabola. Each model was supported at each end in floor-mounted stanchions rather than being attached to the sting-mount arrangement as in the initial test. For two modules,
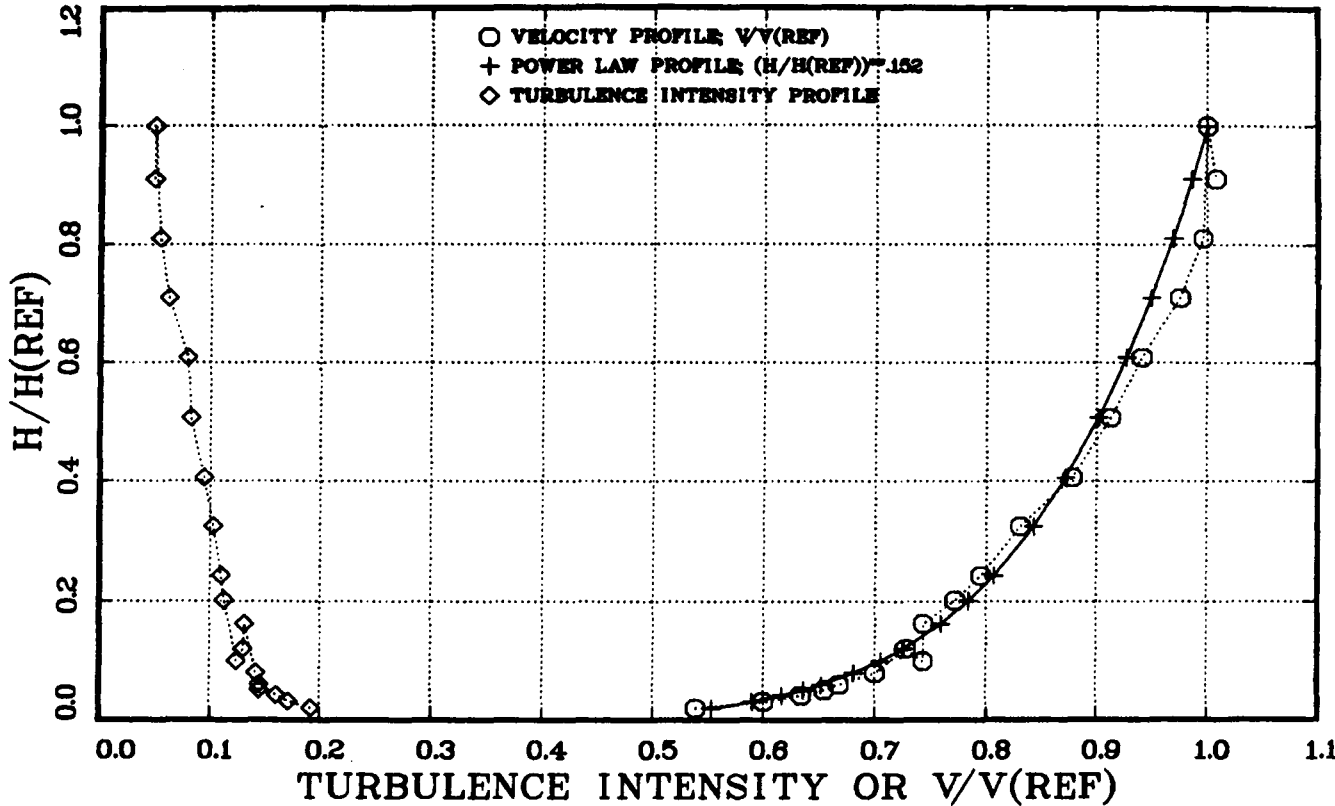
**Figure 1.** Boundary-Layer Flow Profiles

the support stanchions used friction collars around the torque shaft to secure the models at the selected pitch attitude. The third (or metric) model was mounted in ball bearings at the supports, and the torque shaft was attached through an extension to a torque transducer located outside of the support stanchions. The model configuration and test arrangement are illustrated in Figures 2 and 3.

In addition to wind-tunnel dynamic pressure, model torque about the pivot axis was the only other data channel provided.

A Lebow Model 2102-500 strain-gage reaction-torque sensor with a range of ± 500 in.-lb was attached to the torque shaft of one of the parabolic-trough solar-collector models for the purpose of measuring pitching moment. The strain gage was calibrated in place prior to the wind-tunnel test. The strain-gage output signal was fed into an instrumentation amplifier that, in turn, fed amplified output signals to visual digital readouts, an oscillograph recorder, and an analog tape recorder. The oscillograph recorder was used for on-site data presentation. The analog tape record was later digitized for final data reduction.
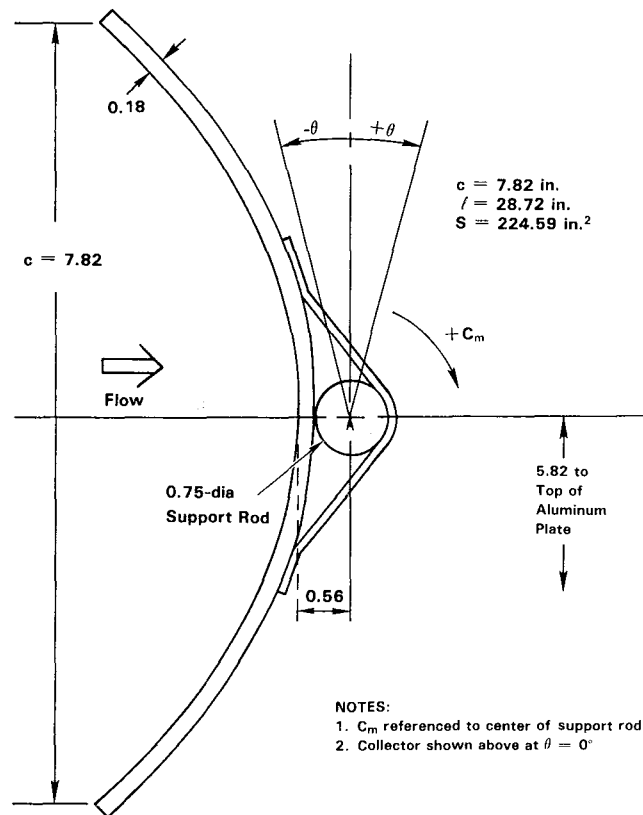


**Figure 2.** Sign Convention—Solar Collector

**Figure 3.** LTV Test Setup
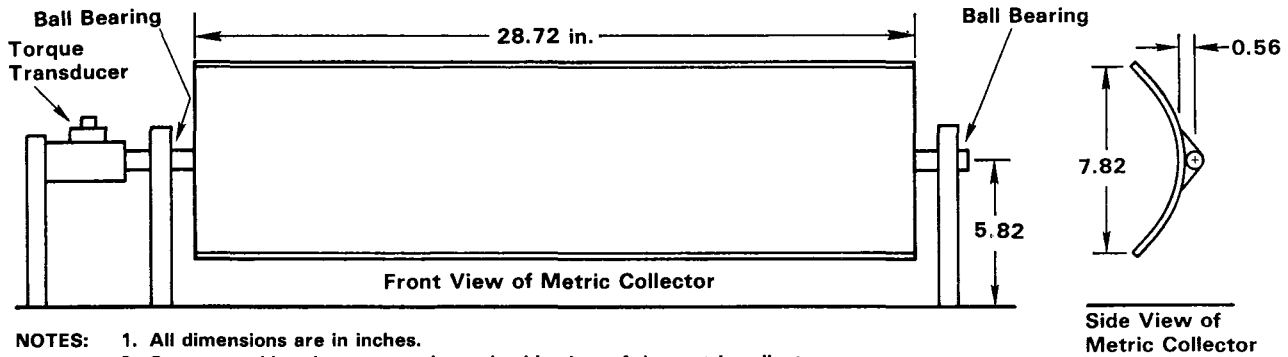
NOTES:
1. All dimensions are in inches.
2. Support and bearing are not shown in side view of the metric collector.
3. Moment coefficients are based on collector area (28.72 × 7.82 = 224.59 in.$^2$, aperture width of 7.82 in., and free-stream dynamic pressure (q) at the collector center line, 5.82 in. above the floor.
4. Moments were measured about the shaft center line, 0.56 in. behind the center of the collector front surface.
5. The torque transducer was mounted on the center collector and the others were uninstrumented.
6. Mounting of the forward and aft collectors was the same as the center one except that friction collars replaced the bearings.
7. Collectors were 2.25 apertures (17.60 in.) apart. The forward collector was 3.00 apertures behind the fence.
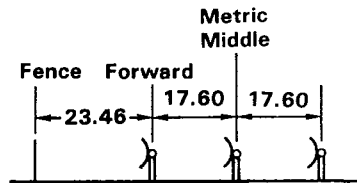
Five model configurations were run during TEST I. These configurations are defined as 0 through IV in Table 1. In TEST I, a collector row consisted of only one collector module.

## 2.3.2 TEST II (CSU)

Up to 18 collector modules from the original CSU test were reused to provide array configurations with nominally three modules per row. With one exception, all modules were reused in their original floor-mounted support struts. A double nut on the pivot shaft at each end of the parabolic trough permitted the model to be secured to the supports at the desired attitude. One module had new pivot shafts fabricated and attached to each end of the parabolic-trough section. These pivots were supported in ball bearings mounted in stanchions attached to an aluminum base plate. Two sets of pivot shafts were provided and offered two alternate pivot-center locations with respect to the vertex of the parabolic section. The full three-module row containing the metric module and the wind-tunnel balance for sensing model torque were mounted to this base plate to reduce alignment problems between the metric module, the torque shaft, and the roll balance. The other five collector rows, comprising the full array, were mounted to individual plywood strips to facilitate changes in the collector array model.

Figures 4 and 5 show a sketch of the collector modules and the array layout. The torque shaft connection between the metric module and the balance required that the right-end module in the metric row be displaced slightly rearward to avoid interference. Even with this displacement, interference can be avoided only within a narrow band of pitch angles at ~0° and 180° orientations. For pitch angles outside these bands, it was necessary to delete the right-end module from the array.
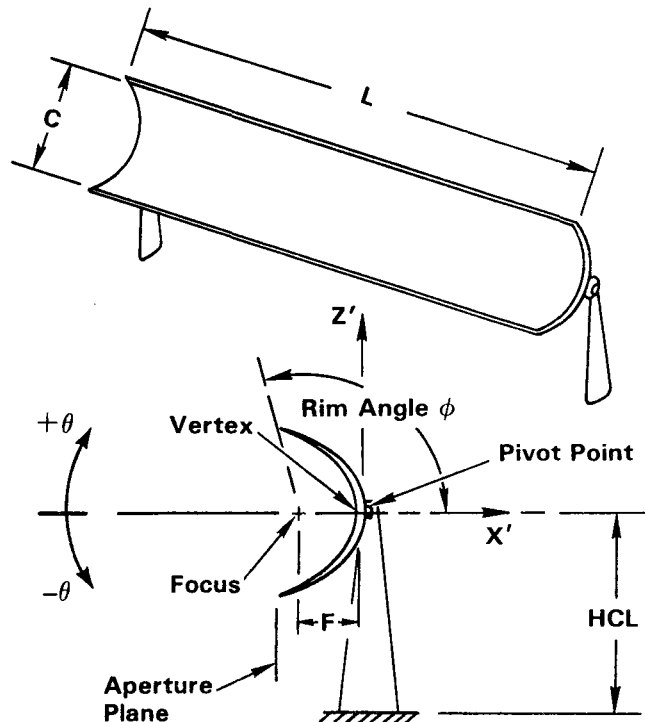


**Figure 4.** Parabolic-Trough Collector Model

10

## Table 1. Collector Array Configurations

| Configuration No. | Description of Collector Array Model |
|---|---|
| 0 | A single isolated collector module (TEST I only) |
| I | Metric collector row + 1 row downstream (TESTS I and II) |
| II | Two collector rows (Conf. I) + an upstream fence (TESTS I and II) |
| III | One collector row upstream + metric row + 1 row downstream (TESTS I and II) |
| IV | Three collector rows (Conf. III) + an upstream fence (TESTS I and II) |
| V | Four collector rows upstream + metric row + 1 row downstream (TEST II only) |
| VI | Twelve collector modules upstream + metric module (TEST II only) |
| VII | Metric collector row + 1 row downstream (TEST II only) |

For TEST I, rows were one collector module per row.

For TEST II, Conf. I through V rows were three collector modules per row; however, an asterisk superimposed ahead of the Conf. number (*I) indicates the right-end module in the metric row was removed to preclude interference with the torque shaft.

For TEST II, Conf. VI and VII, rows were one collector module per row.

First letter following Conf. No. designates pivot center location.
    A Pivot Center = 0.0716 aperture widths behind parabolic vertex
    B Pivot Center = 0.0212 aperture widths behind parabolic vertex
    C Pivot Center = 0.0698 aperture widths ahead of parabolic vertex

Second letter designates fence configuration.
    A Porosity = 40% (perforated sheet stock with 1/8-in.-dia holes)
    B Porosity = 23% (perforated sheet stock with 3/8-in.-dia holes)
    C Porosity = 68% (copper wire screen supported on rods simulating a chain-link    type fence)

Arabic numeral designates fence spacing in aperture widths (C) upstream from first collector row.

Example: *IIBA1.5 designates a two-row array, metric + downstream row with the right-end collector in metric row removed. Pivot center located 0.0212 (C) behind vertex with a 40% porosity fence located 1.5 (C) upstream from metric row.
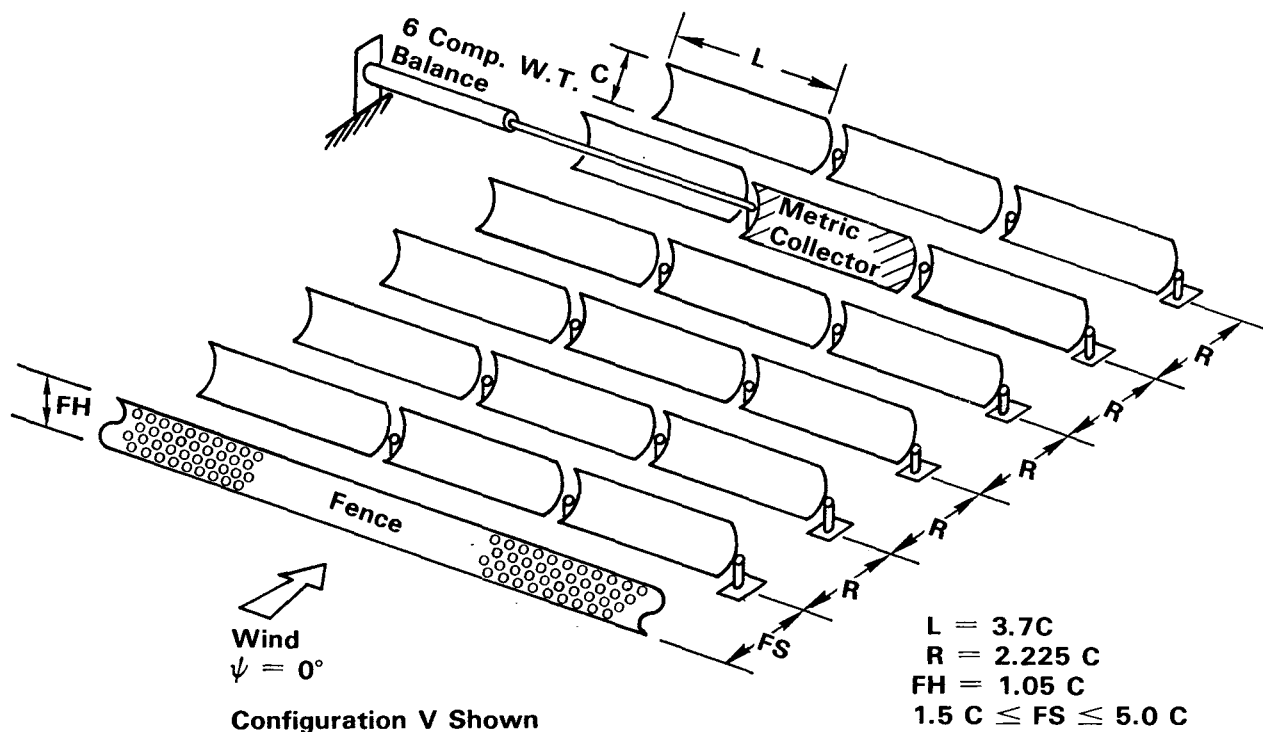
**Figure 5.** Array Model Layout

Three different fence configurations were evaluated. Two of these fences were fabricated from perforated sheet stock with hole size and spacing that resulted in porosities of 23% and 40%. The third fence configuration was made up of 20-mesh copper screen supported on a 1/8-in.-dia brass-rod framework simulating a chain-link fence installation. The wire screen material provided a 68% porosity. Fence height for all configurations was 1.05 apertures. Fence spacing upstream from the perimeter collector row varied from 1.5 to 5 collector aperture widths.

An SNLA six-component, strain-gage, wind-tunnel balance was used as the load-sensing element.

Model torque was measured on the roll gage of this balance; however, load interactions appearing on the other component gages were monitored and used as inputs to the data-reduction matrix developed during pretest calibration procedures. In all cases, the interaction contributions turned out to have an insignificant contribution to model pitching moment. Rolling moment range for this balance is ±5 in.-lb. The same signal conditioning, recording, and readout equipment used for the LTV test were also used here. Array configurations tested are delineated in Table 1.

# 3. Data Reduction and Presentation

Three coordinate axis systems are useful in describing wind-induced loads on parabolic-trough solar collectors. These three systems (the wind axes, foundation axes, and body axes) are illustrated in Figure 6. To the collector system designer, forces and moments expressed in the foundation-fixed axes are of primary interest. In these systems with the trough at 0° "pitch angle" and 0° "yaw angle," wind blowing into the concave trough is moving in a positive direction along the X (and X′) axis; the Z axis is perpendicular to the wind and earth (positive upward), and the Y axis coincides with the parabolic vertex of the trough to provide a right-hand rule axis system. A positive yaw angle results from rotating the collector module in a positive (right-hand rule) direction about the Z axis

relative to the wind vector. Thus, the wind axes are obtained from the foundation axes through a rotation about the Z axis equal to the yaw angle $\Psi$ so that the X axis coincides with the wind vector. A positive pitch angle results from rotation of the parabolic trough in a positive (right-hand rule) direction about the Y′ axis. Body axes, being fixed with respect to the parabolic trough, are related to the foundation axes through an angular rotation equal to the pitch angle $\theta$.

During both of the tests reported here, a direct measurement of the torque about the collector pivot axis was made. In both cases, however, the collector pivot axis was displaced from the Y′ axis laterally along the X″ axis. Ordinarily, such translation of the moment center away from the coordinate axis poses
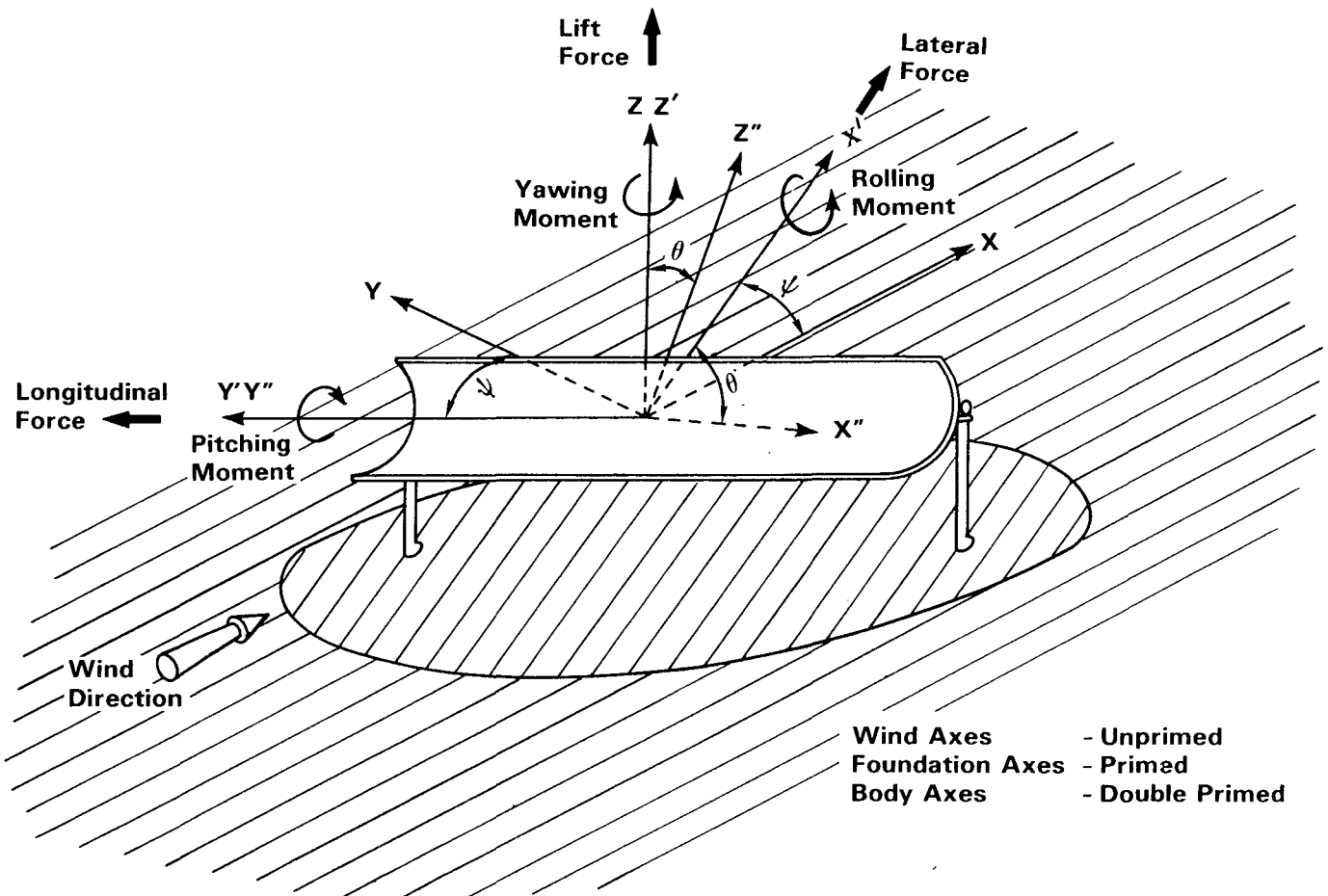


**Figure 6.** Coordinate Systems

13

no problem, since a knowledge of the collateral resultant force acting in the plane perpendicular to the pivot axis (and the parallel coordinate axis Y′) permits calculation of an equivalent moment at alternate pivot centers. However, during both tests, the pitching moment was the sole load measured. Therefore, without a knowledge of the accompanying simultaneous lateral and lift forces, the moment data must be associated with the respective pivot center used, and computation of equivalent values for alternate pivot axes becomes impossible. For TEST I, the collector pivot axis was located 0.0716 collector apertures behind the parabolic vertex (Figure 2). During TEST II, moments were measured about two pivot axis locations: 0.0212 aperture widths behind the vertex and 0.0698 aperture widths ahead (toward the parabolic focus) of the vertex.

Because of the turbulent nature of the flow, especially during TEST II, data was recorded over an extended time period and mean values of the pitching moment computed. Output from the load sensor was recorded on magnetic tape for posttest reduction. This analog record was sampled periodically and progressive mean values of the pitching moment coefficient computed from a sample size that was gradually enlarged by the inclusion of successive data samples until it finally included the entire run interval. The results of this process are illustrated in Figures 7A through 7C for three configurations run during TEST I. The TEST I data was sampled at a rate of 10/s over a 15-s run interval. A similar procedure was used in reducing the TEST II data with the exception that a sample rate of 4/s over a 100-s run interval was used. Analogous results for TEST II are presented in Figures 8A through 8C. The data from both TESTS I and II indicate that the mean value of the coefficient has attained a stable asymptote within the initial third of the run interval. Furthermore, the data substantitate the significantly lower turbulence level existing in the LTV tunnel airflow.



(A)
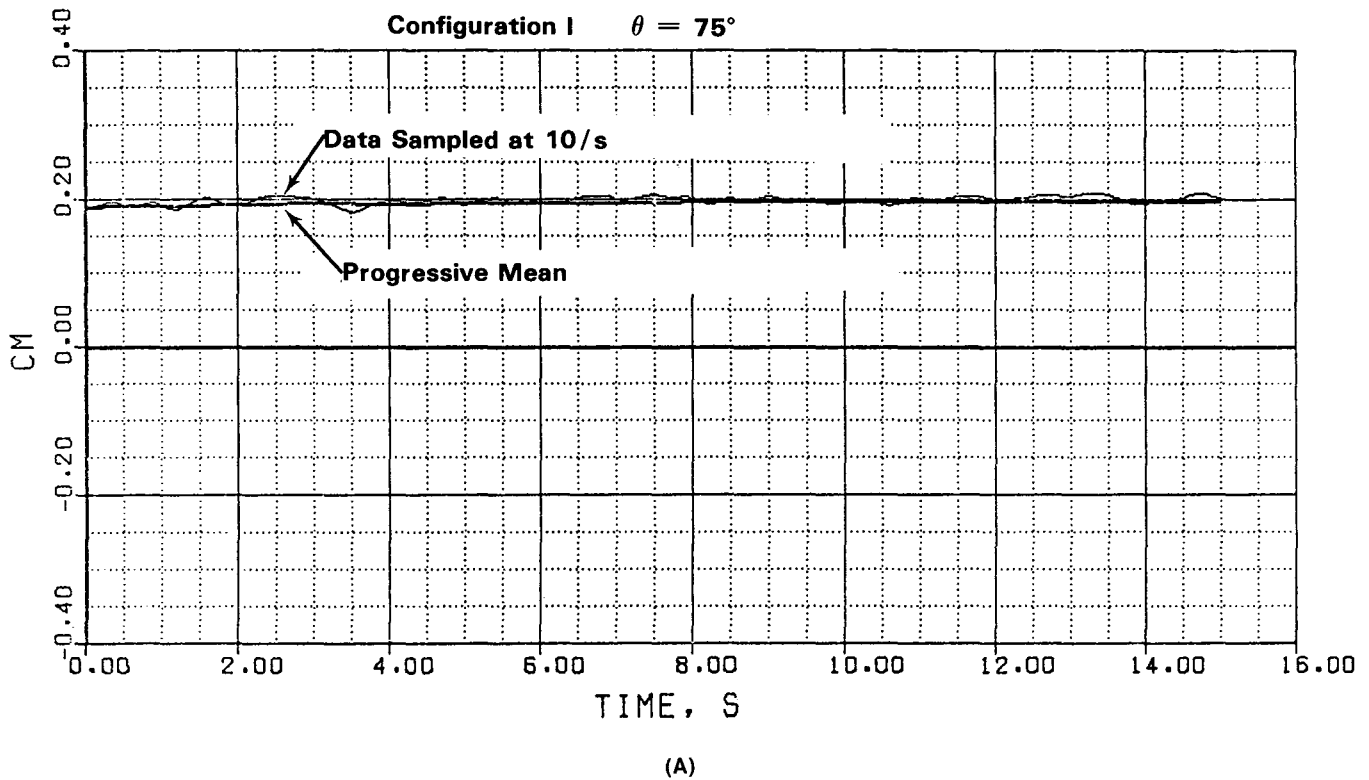
Figure 7. Record of Sampled Data, TEST I

14

Configuration III    θ = 75°

(B)



Configuration IV    θ = 45°

(C)
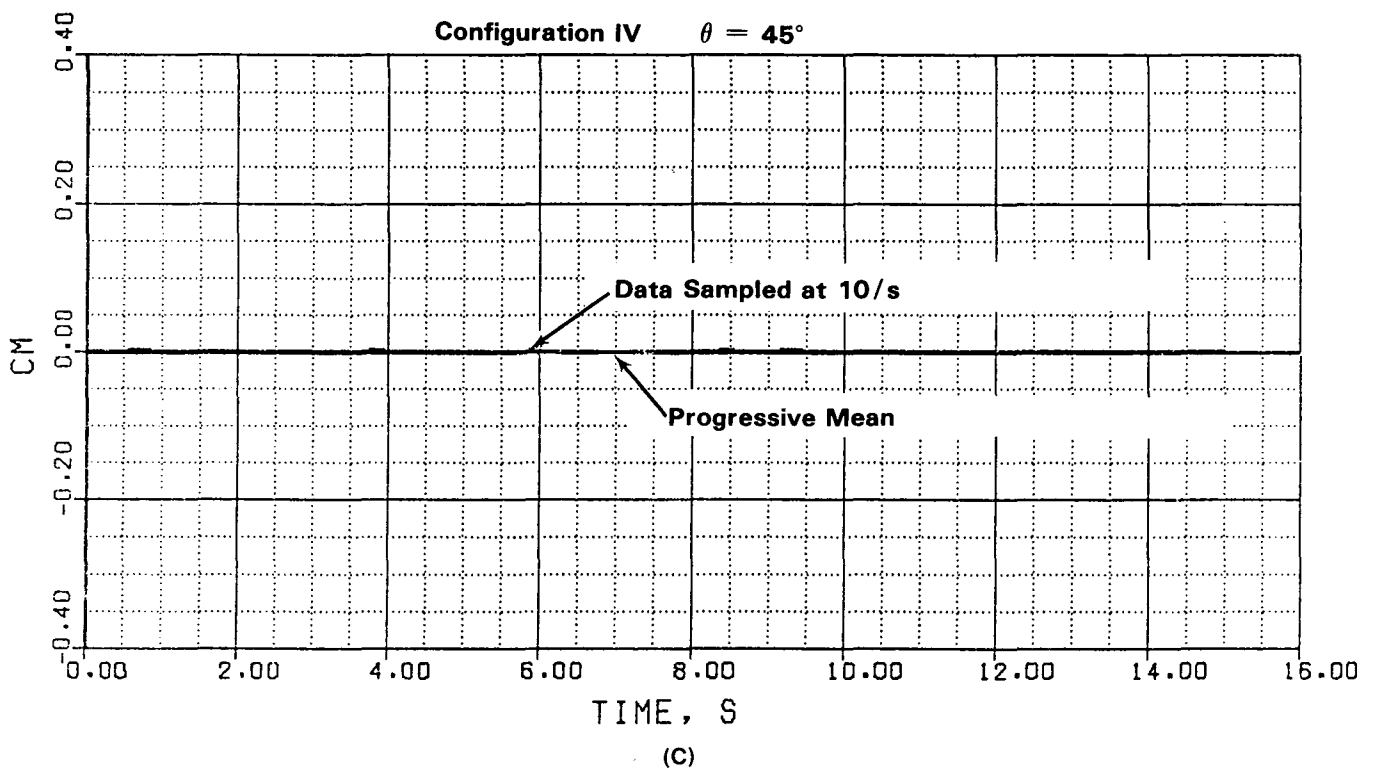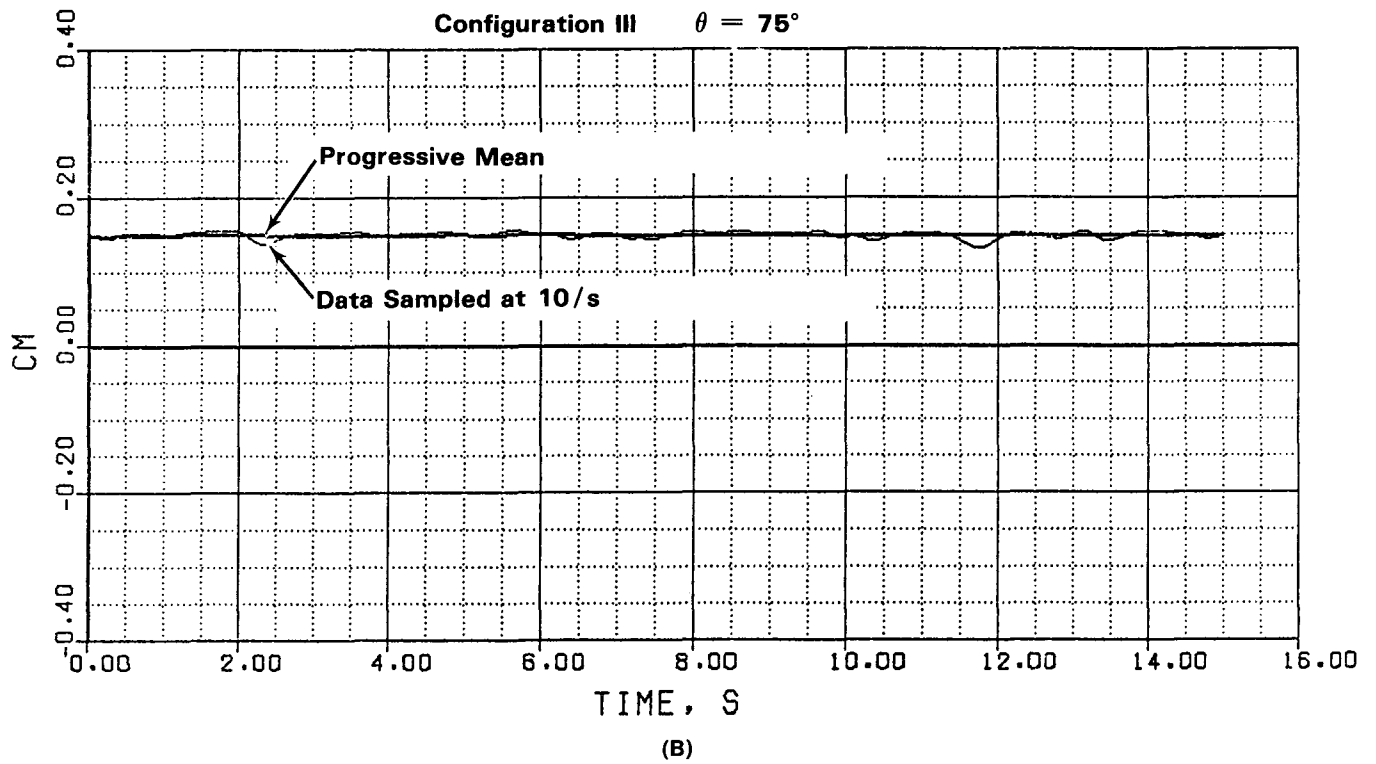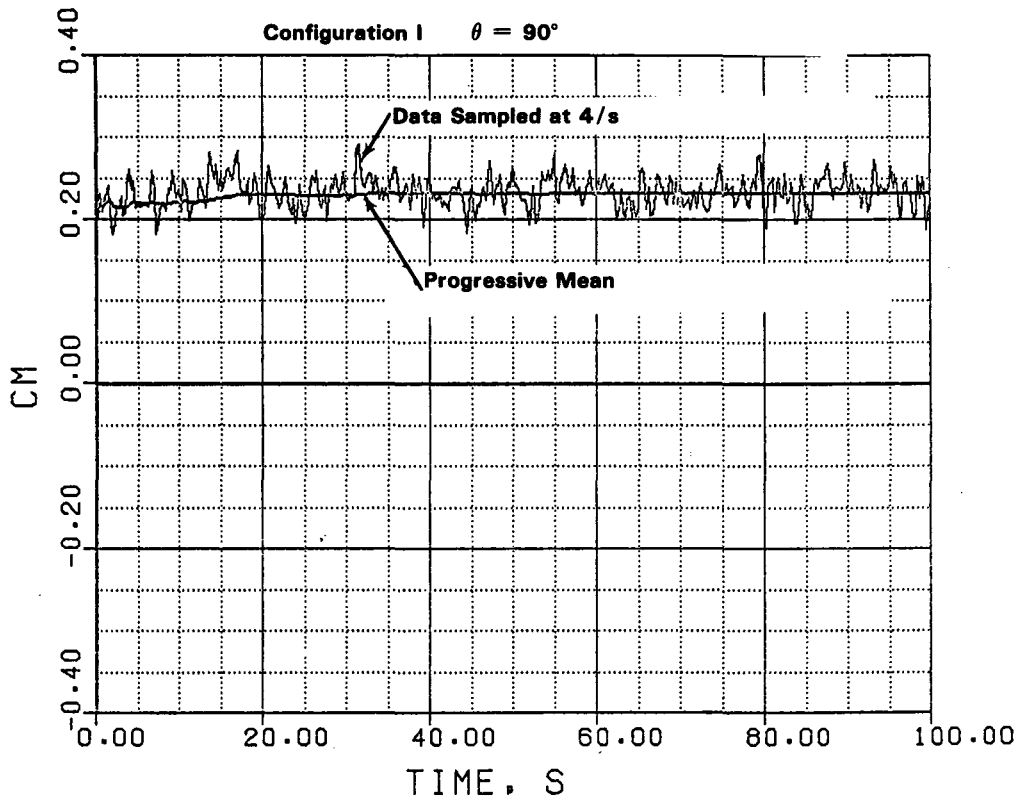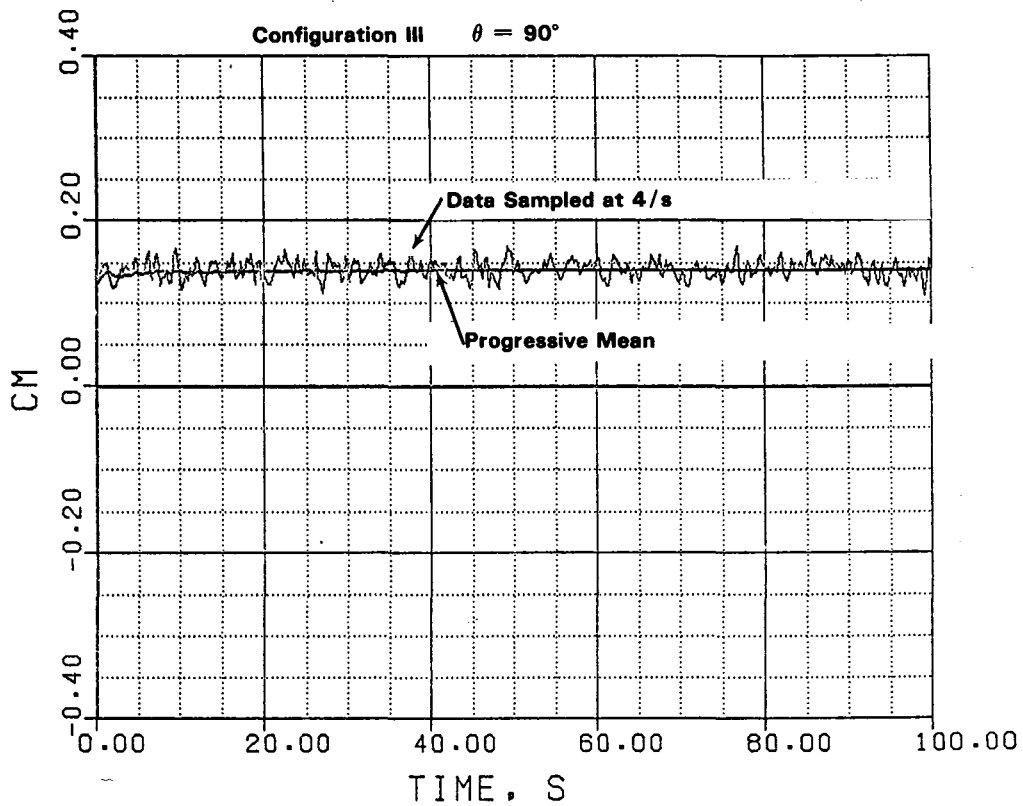
Figure 7 (concluded)

Figure 8. Record of Sampled Data, TEST II
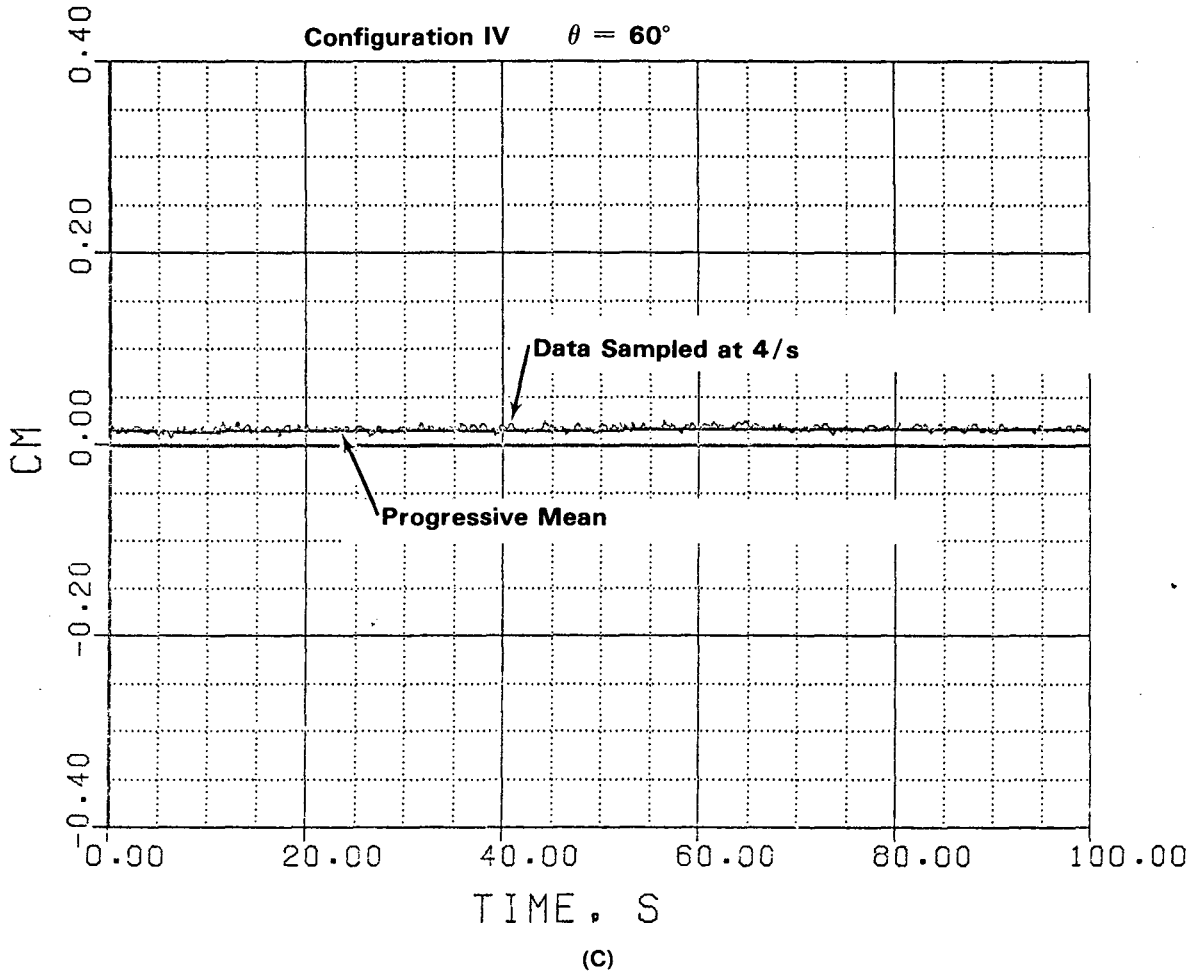
**Figure 8 (concluded)**

The moment measured on the trough models was reduced to nondimensional coefficient form in accordance with Eq (1)

$$C_{m_\theta} = \frac{\text{MOMENT}(\theta)}{qA\ell} \qquad (1)$$

where

dynamic pressure $q = 1/2 \, \rho \, V_H^2$

$\rho$ = mass density of flow

$V_H$ = free-stream velocity at trough centerline elevation

reference area $A = C \times L$

reference length $\ell = C$

$C$ = trough aperture width

$L$ = trough length

In accordance with the laws of dynamic similarity, these coefficient values may be extrapolated to the full-scale situation when flow regime and Reynolds number equivalency prevails between the model and full-scale situation. It was demonstrated in Reference 2 that parabolic-trough collector loads appear relatively insensitive to the Reynolds number within the relevant range of model to full-scale values. Therefore, one may use the experimental coefficient values developed here to estimate full-scale loads by inverting Eq (1) and using the appropriate full-scale values for dynamic pressure and the reference area and length.

# 4. Analysis of Test Results

The collector array configurations tested during both TESTS I and II are tabulated in Table 1.

## 4.1 TEST I

Five different array configurations were run during TEST I to evaluate the effect of interference from adjacent fore and aft collector modules or from an upstream fence. Pitching moment coefficient data versus collector pitch attitude are presented in Figure 9 for Configurations 0, I, and III. These data illustrate the effect of adding a collector module downstream and of subsequently adding a third module upstream from the metric module. The data indicate that the presence of the collector module downstream from the metric collector has a minimal influence on the moment characteristics; a slightly smaller magnitude at both the positive and negative peaks is the only disparity between Configurations 0 and I. The lack of intervening data points between 0° and 90° pitch for Configuration 0 causes the computer- drawn curve to reflect an erroneous trend. Were intervening data

available between 0° and 90° pitch, the trend would probably correspond to Configuration I.

The presence of the upstream collector module, however, significantly alters the pitching moment characteristics. In addition to significantly reducing the magnitude of both the positive and negative peaks, the upstream collector module alters the static stability characteristics. Whereas Configurations 0 and I exhibit statically stable trim angles

$$\left( \frac{dC_m}{d\theta} < 0 \ @ \ C_m = 0 \right)$$

at ~0° and ±180° and unstable trim angles at approximately ±70°, the presence of an upstream collector results in regions of neutral stability between pitch angles of -45° to +45° and -135° to -150°, and only one statically stable trim angle at approximately 125° pitch.

The effect of adding a fence upstream is illustrated in Figures 10 and 11. Figure 10 presents results for the addition of the fence upstream from the metric
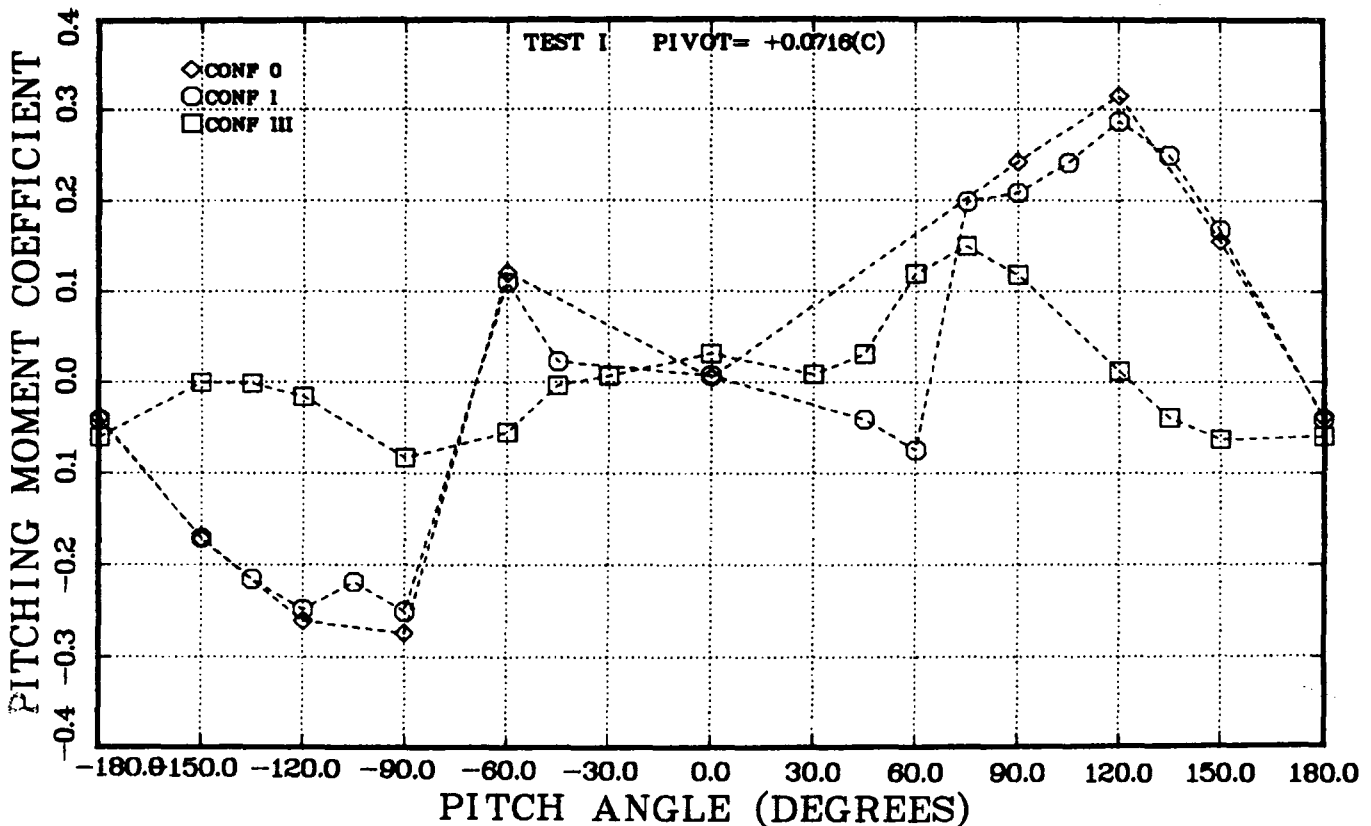


**Figure 9.** Pitching Moment vs Attitude for Configurations 0, I, and III

collector (representing perimeter row collectors); Figure 11 represents results for collectors in the second row of an array behind a fence. In both cases, the fence provides a very significant reduction in the pitching moment characteristic over the entire pitch-angle range. During TEST I, only a single fence configuration was used. This was Fence A (40% of porosity) placed 3.0 aperture widths upstream from the perimeter row of the collector array.

## 4.2  TEST II

After the pitching moment data of TEST I failed to substantiate the analogous data of Reference 2 in the presence of upstream interference, a more comprehensive test was undertaken. A number of parameters related to collector and array configurations were investigated. These parameters include

   a. Influence of intrarow adjacent module on metric module;
   b. Pivot center location on collector module;
   c. Embedded depth of metric module;
   d. Fence spacing upstream from perimeter row;
   e. Fence porosity.

### 4.2.1 Influence of Intrarow Adjacent Module on Metric Module

Whereas, TEST I was conducted using single collector modules to represent array rows, TEST II typically used three collector modules per row with the metric module in the center. Within certain pitch-angle ranges, however, it was necessary to remove the right-end module from the metric row to avoid interference with the torque shaft connecting the metric module to the load balance. Test results with and without the presence of the right-end module are compared in Figures 12A through 12E for selected array configurations. These results indicate that the presence or the absence of the right-end collector module does not significantly influence the metric module pitching moment either with or without upstream interference from array rows or a fence. This result substantiates data[2] that indicated collector modules within a row are aerodynamically independent when intermodule gaps are equal to or greater than 0.06 aperture widths.
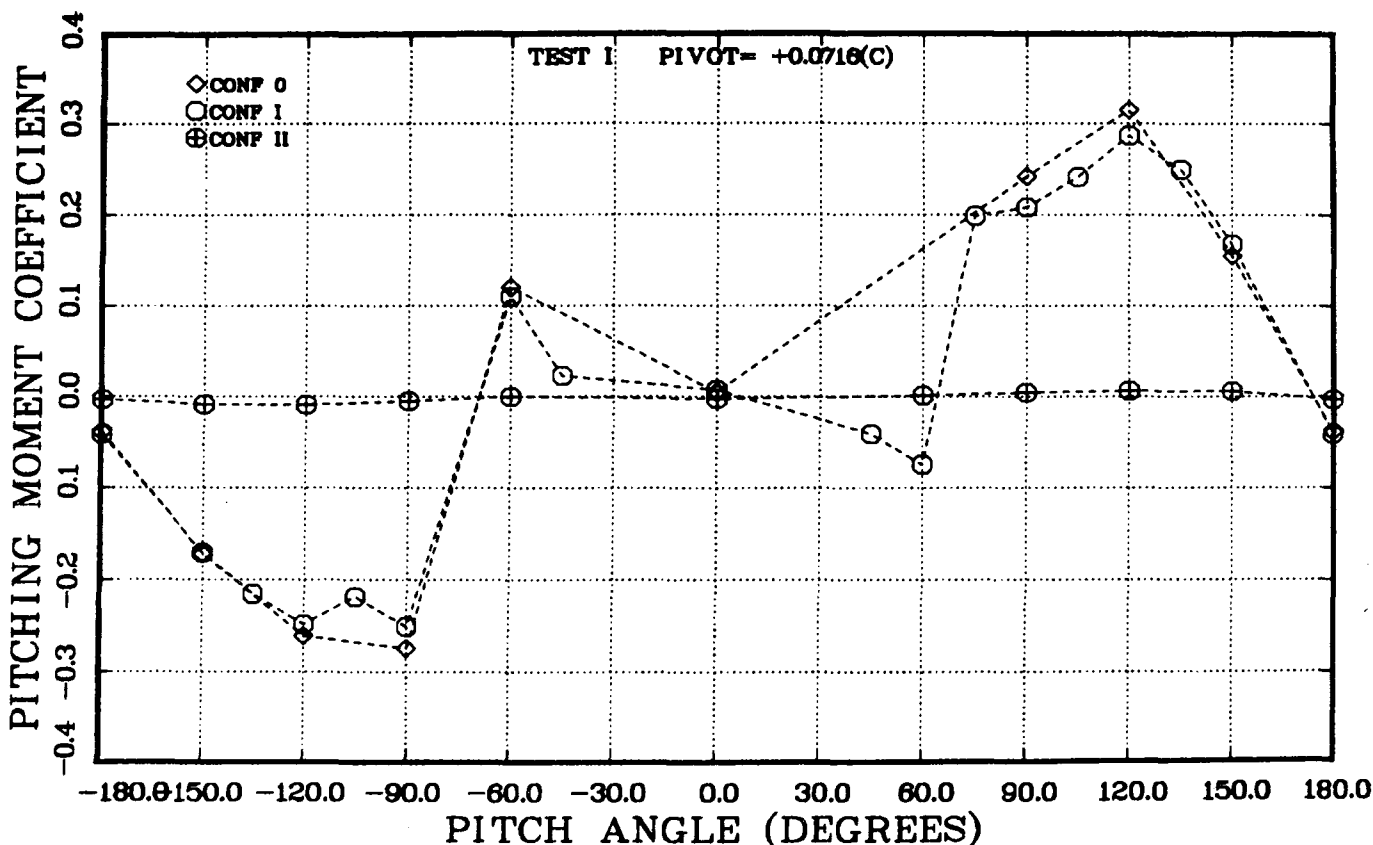


**Figure 10.** Pitching Moment vs Attitude for Configurations 0, I, and II
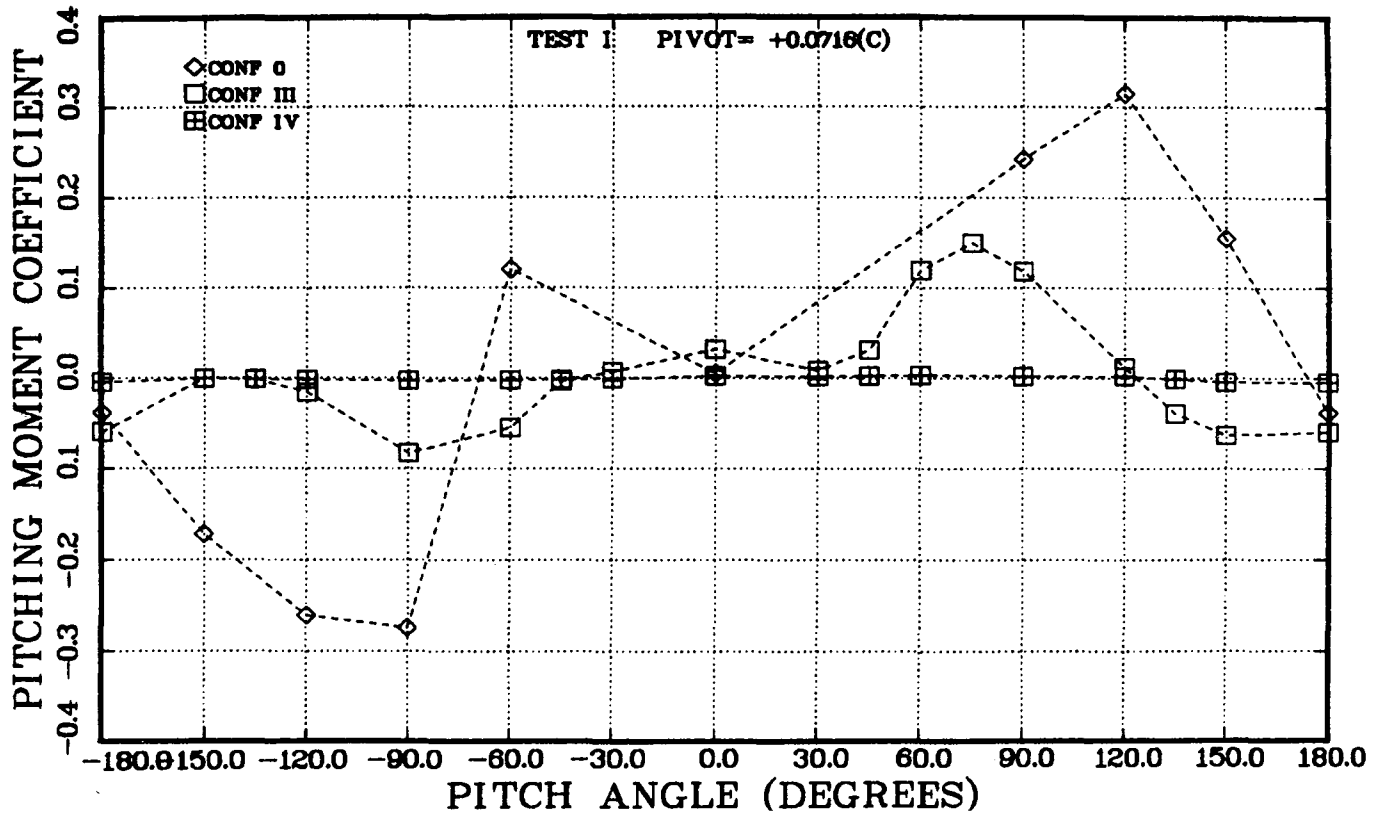
**Figure 11.** Pitching Moment vs Attitude for Configurations 0, III, and IV



(A)
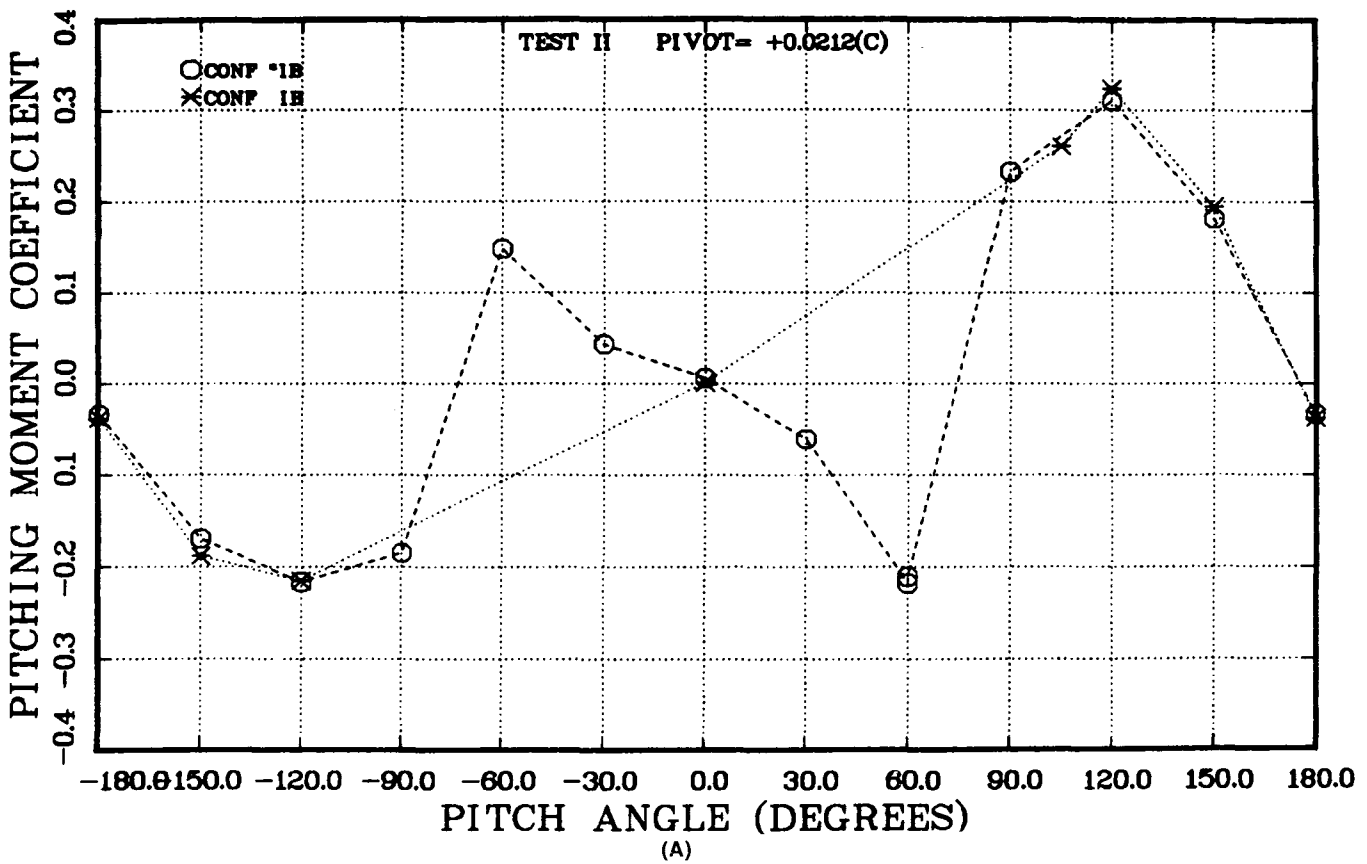
**Figure 12.** Comparison of the Test Results With and Without the Presence of the Right-End Module in the Metric Row

20

(B)



(C)

**Figure 12 (cont)**

21
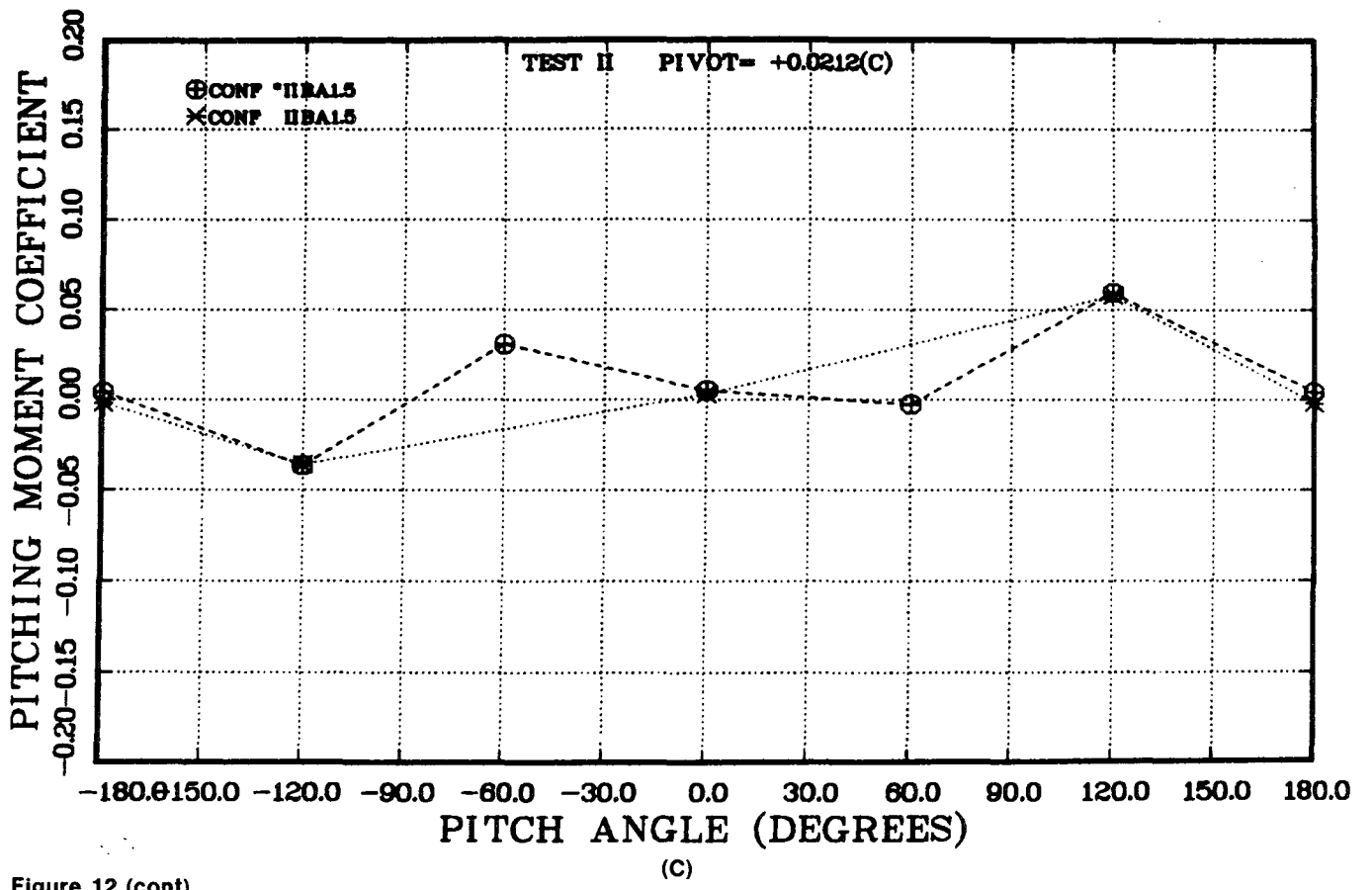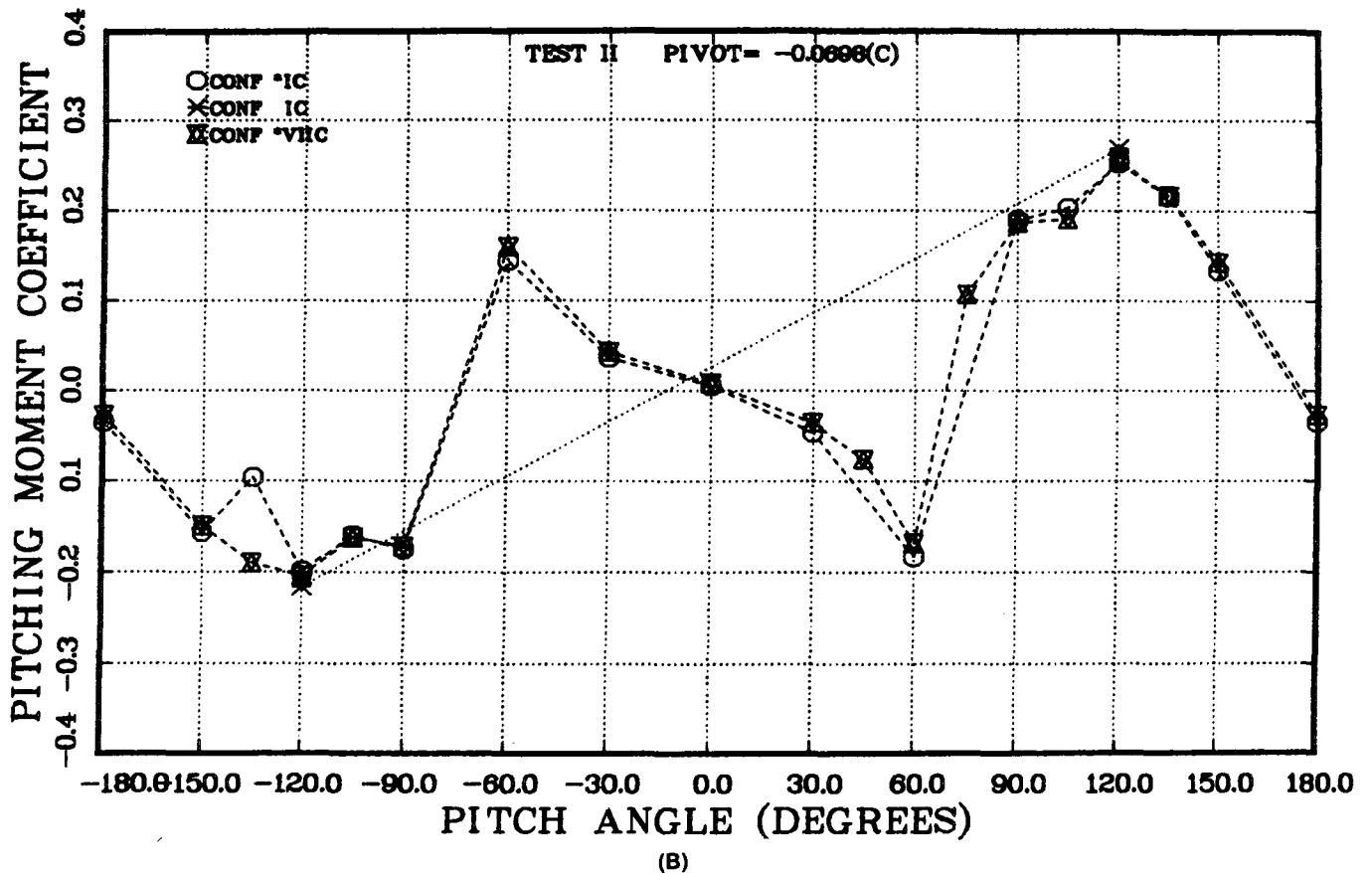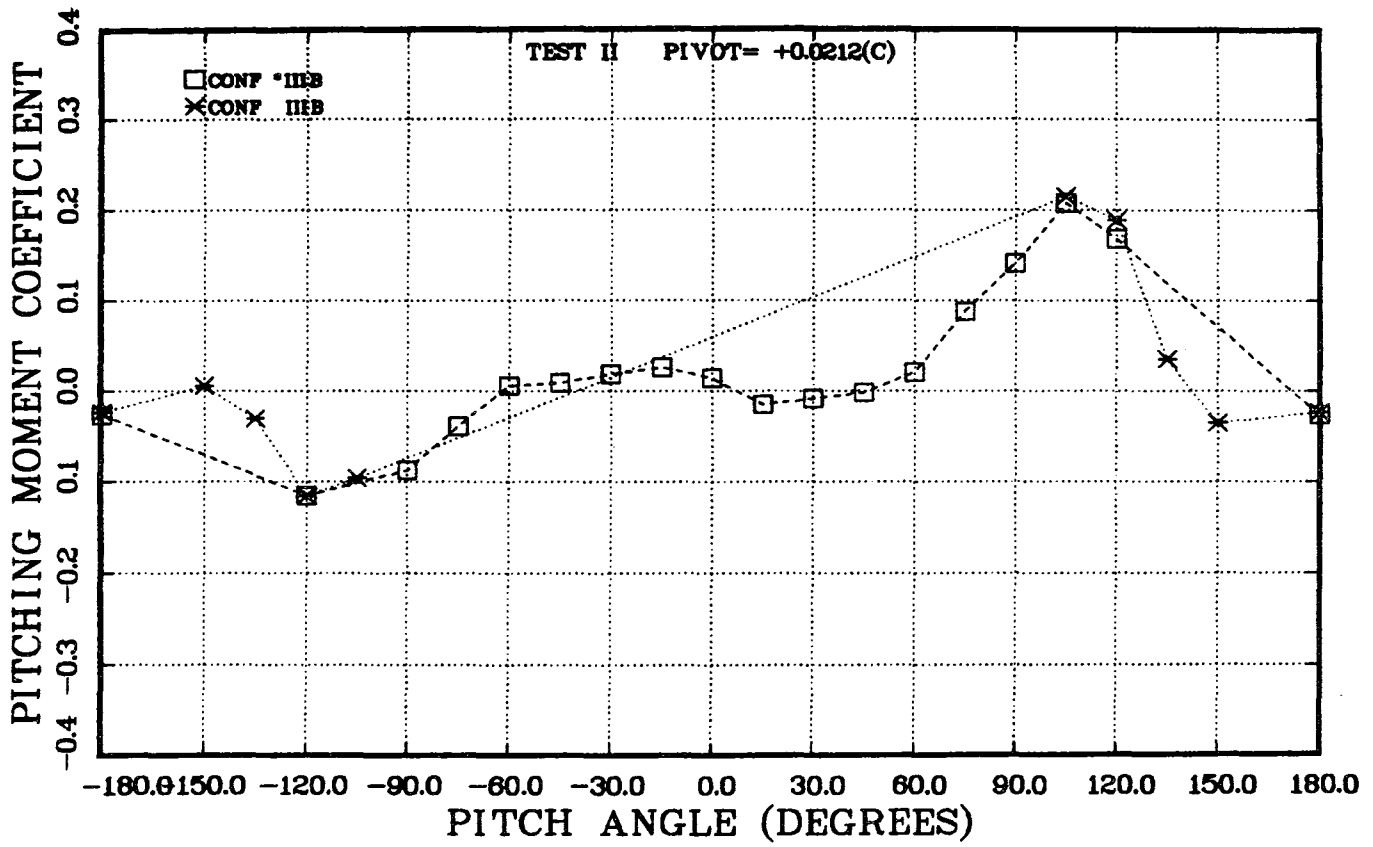
(D)
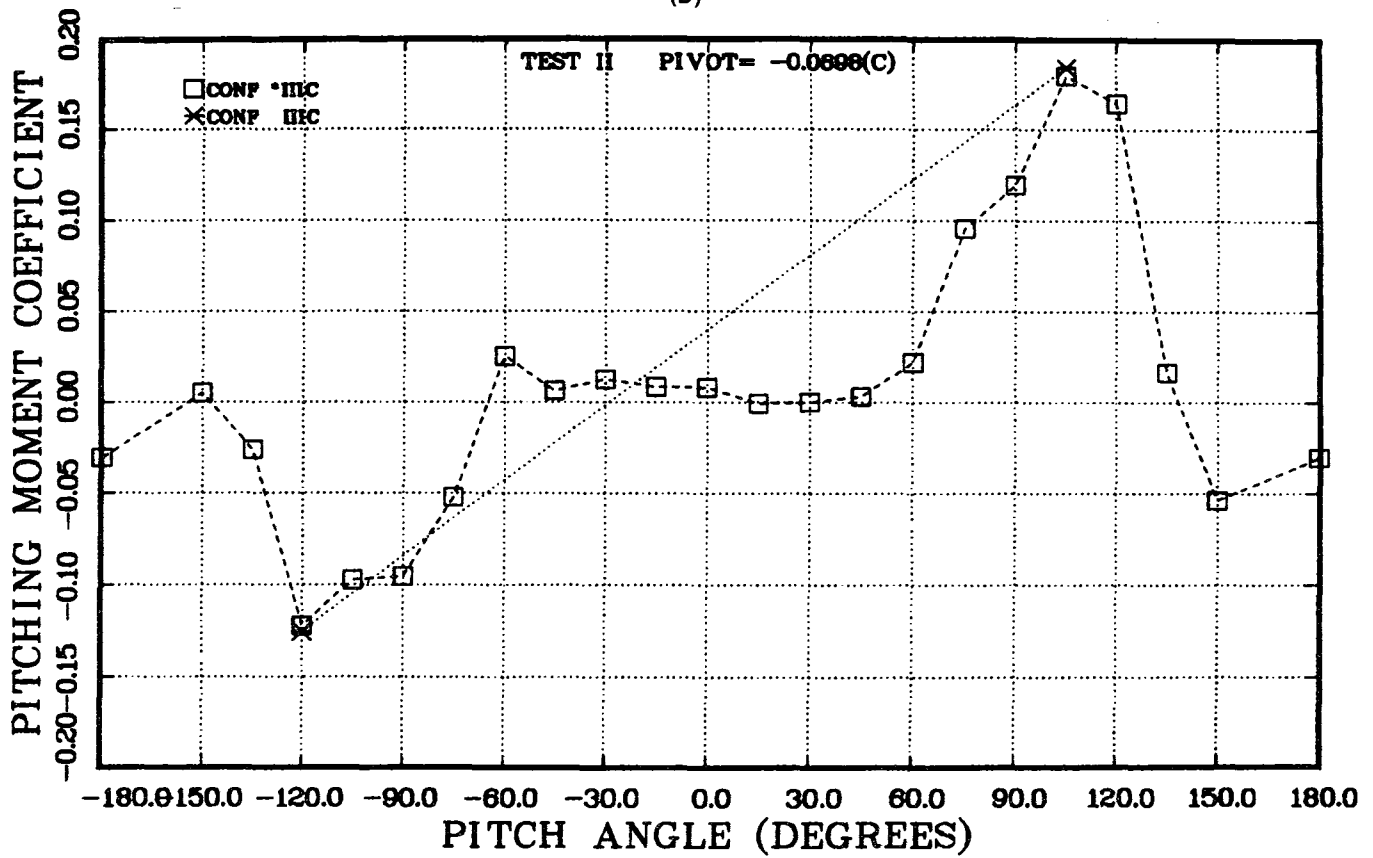


(E)

Figure 12 (concluded)

## 4.2.2 Pivot-Center Location on Collector Module

The influence of pivot-center location is illustrated in Figures 13A through 13F. The lack of collateral force data, together with the measured moments, prohibits transferring these data to equivalent pivot centers for a direct comparison. Theoretical considerations indicate that, as the pivot center is shifted near or to the parabolic-trough center of pressure, the magnitude of the pitching moment should decrease. The experimental data for Configuration I, representing an unshielded perimeter row of an array (Figures 13A and 13B), support this trend for pitch attitudes in the vicinity of the positive peak. Over the remainder of the pitch-angle range, the data for the two pivot centers show few differences. The data for Configuration III (Figure 13D and 13E), representing shielding from a single upstream collector row, reflect a similar trend. A forward shift of the pivot center by 9.1% of the aperture results in an 18% reduction in the peak pitching moment for Configuration I and a 14% reduction for Configuration III. However, as indicated above, this trend does not extend to the negative peak. For shielding provided by an upstream fence, Configurations II and IV (Figures 13C and 13F) demonstrate a similar trend at the peak positive moment. The shielding has reduced the load levels so that data scatter has a more significant effect, making it more difficult to quantify pivot center influence.
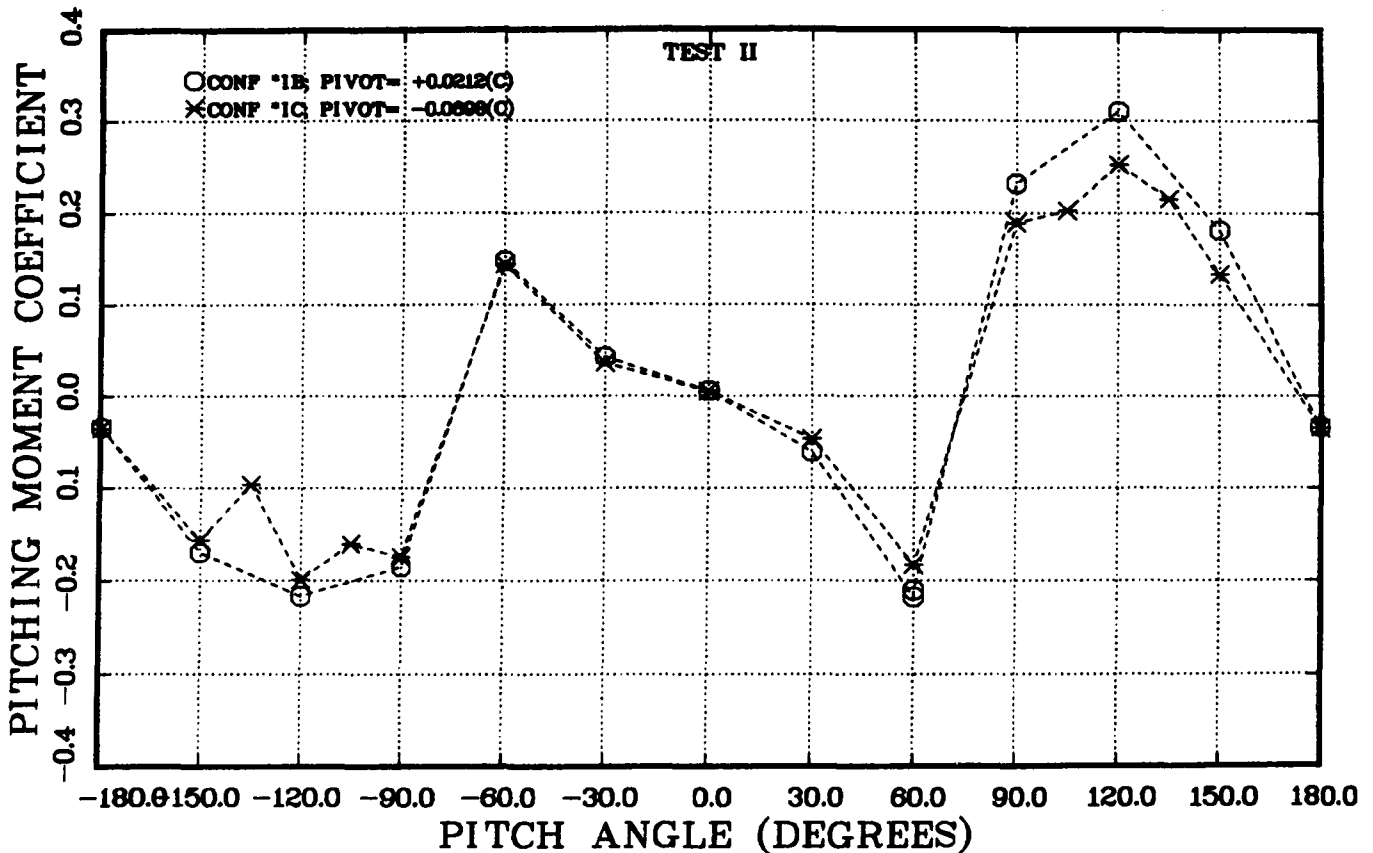


(A)

**Figure 13.** The Influence of Pivot Center Location on Pitching Moment

23
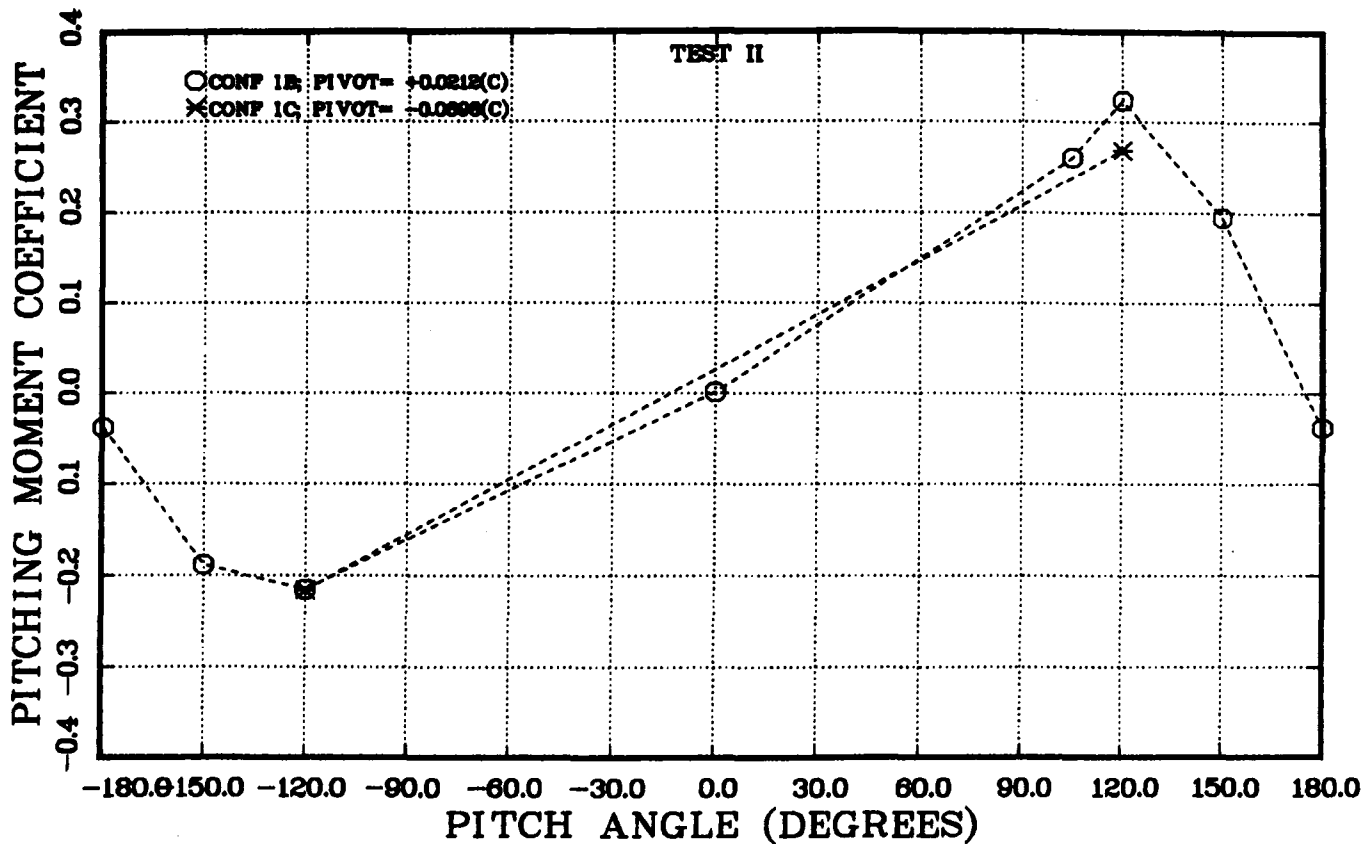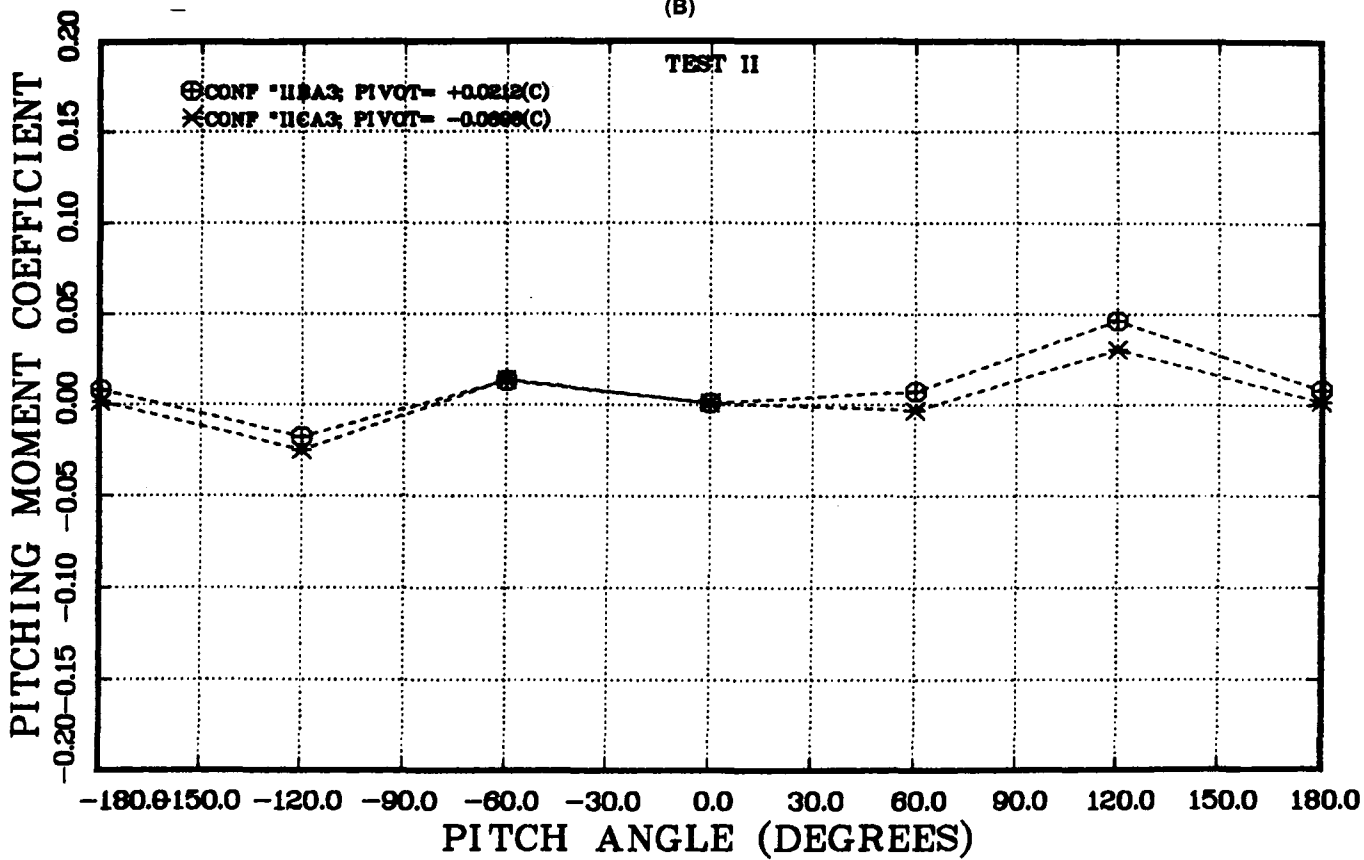
Figure 13 (cont)

Figure 13 (cont)

25
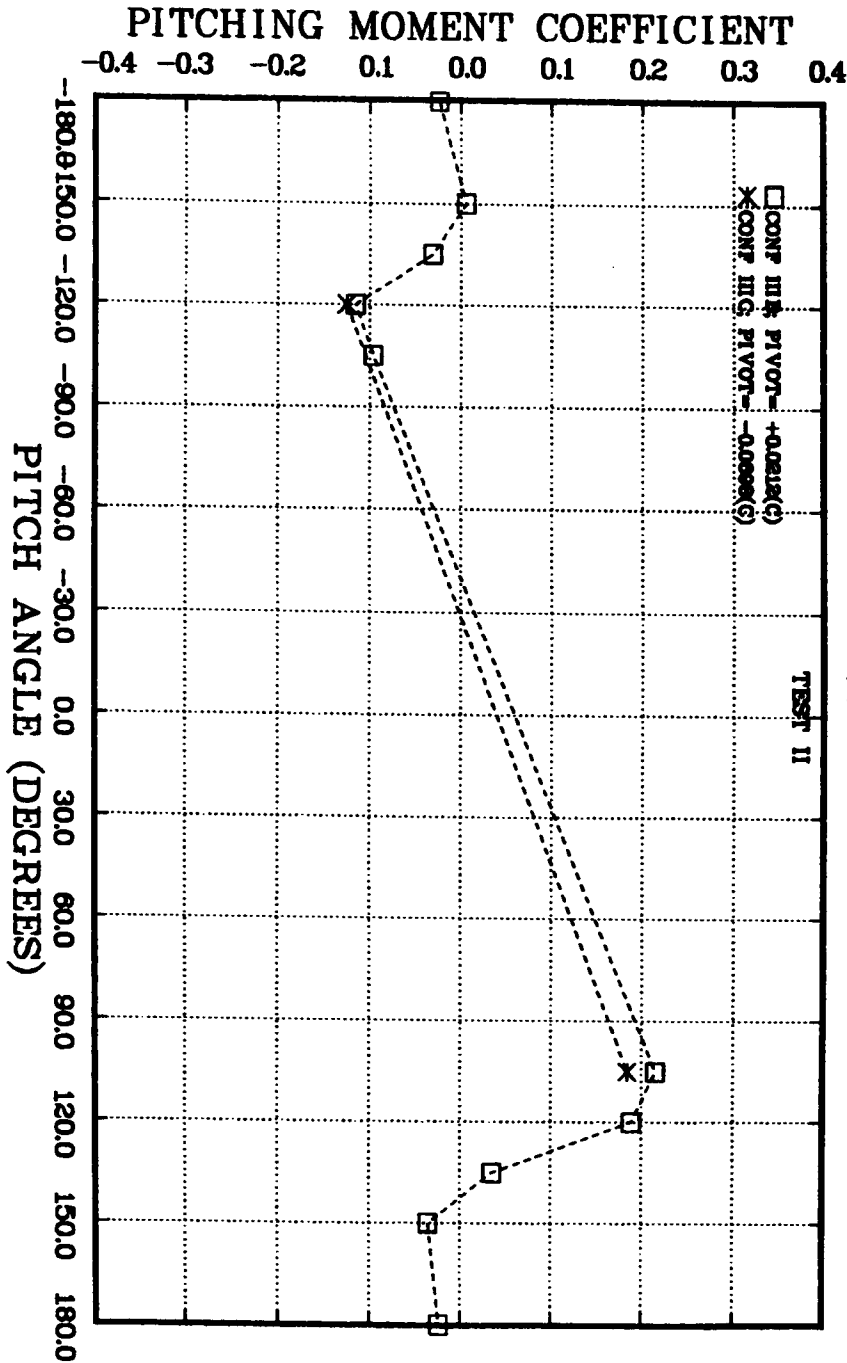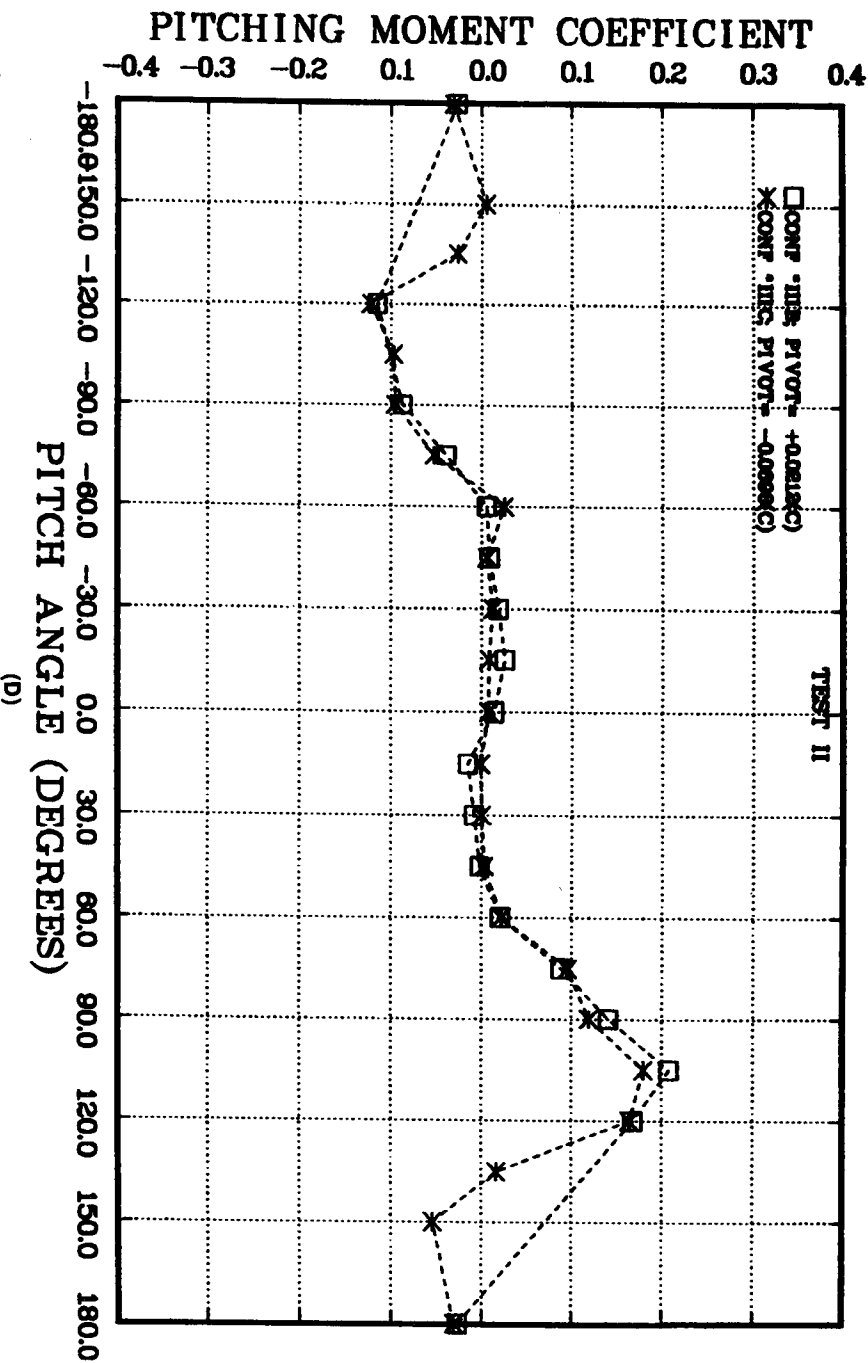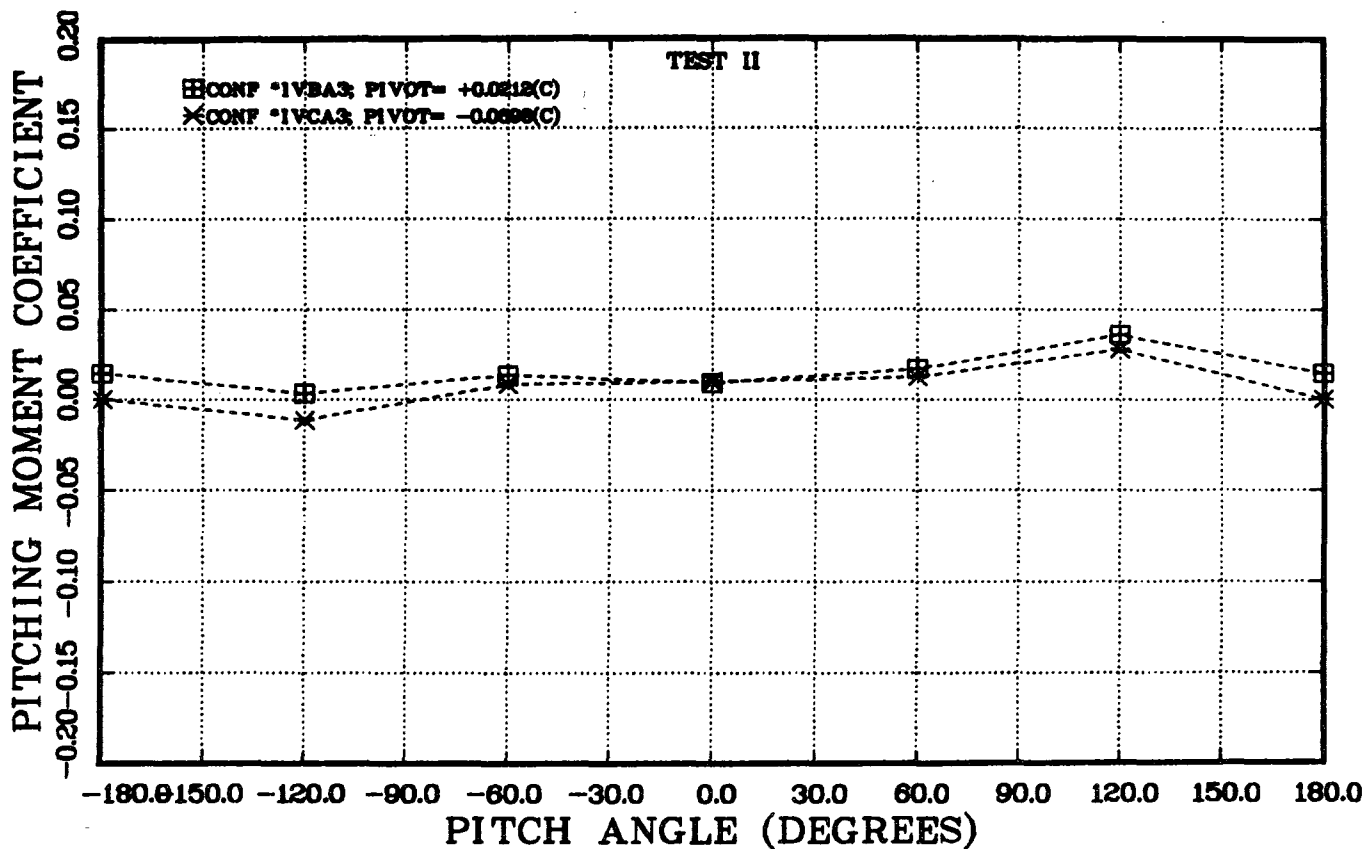
**Figure 13 (concluded)**

## 4.2.3 Embedded Depth of Metric Module

The influence on collector pitching moment characteristics that result from various levels of upstream shielding are illustrated in Figures 14A and 14B. The progressive reduction occurring in the peak pitching moment as a result of adding upstream a single collector row, four collector rows, and, finally a fence plus the four rows are illustrated in Figure 14A. The pitching moment experienced by a collector module embedded at various row depths within an array and protected by a 40% porous upstream fence is shown in Figure 14B. Configuration VI (included here) represents the downwind perimeter row of an array. The reader should be aware that this configuration did not have

the fence across the downstream end of the array, thus allowing flow reattachment to the tunnel floor (ground) nearer to the downwind perimeter row than is otherwise likely. The moment reductions afforded by fence configurations of 23% and 40% porosity to the first and second rows of an array are illustrated in Figures 15A and 15B, respectively. Similar data for the alternate pivot-axis location and for the 40% and 68% porosity fences are shown in Figures 16A and 16B. These data indicate that increasing levels of upstream shielding lead to progressively reduced peak pitching moments. In all cases, the presence of a 23% or 40% porous fence provides a reduction in peak pitching-moment characteristics to less than one-third the corresponding unshielded value.
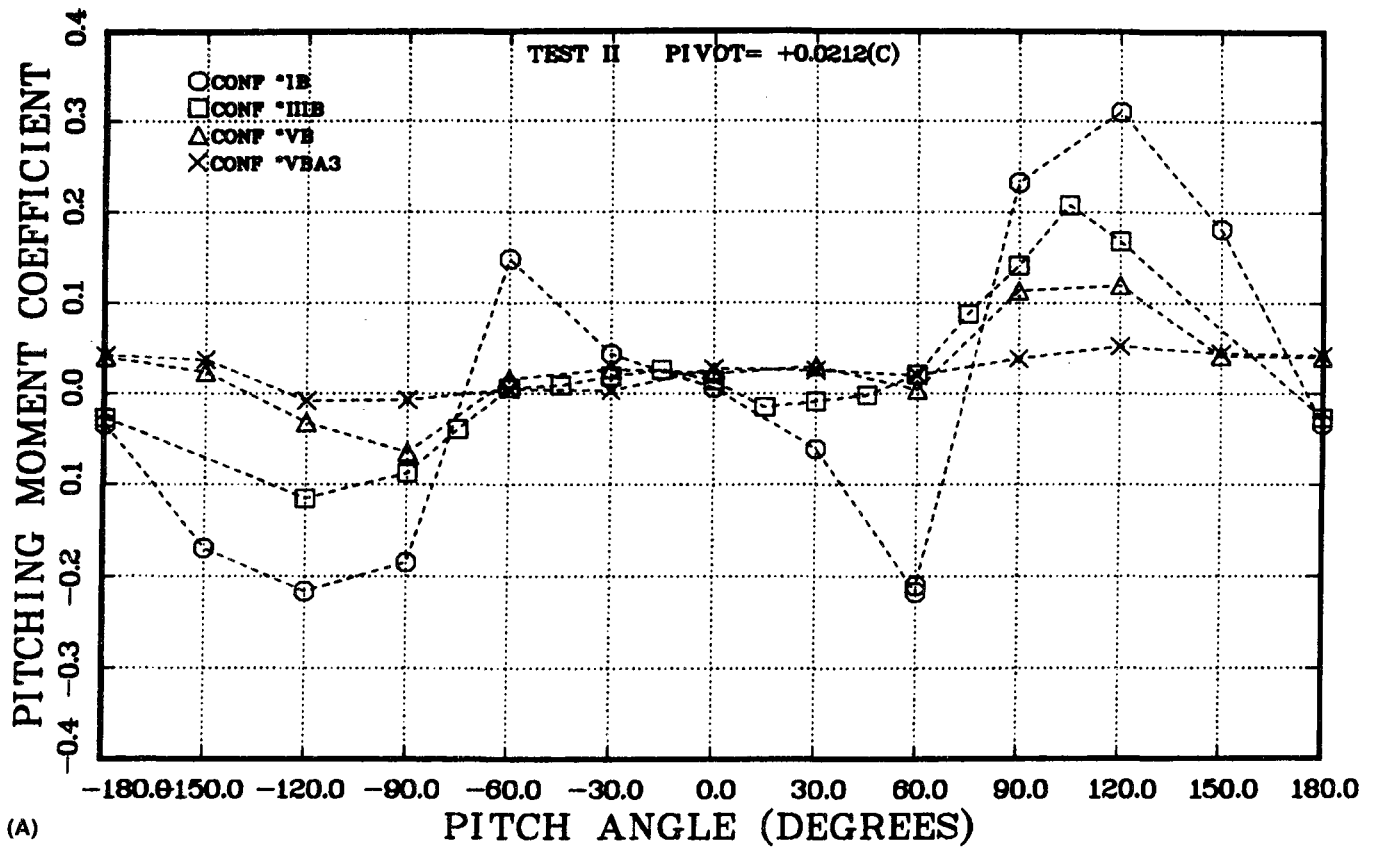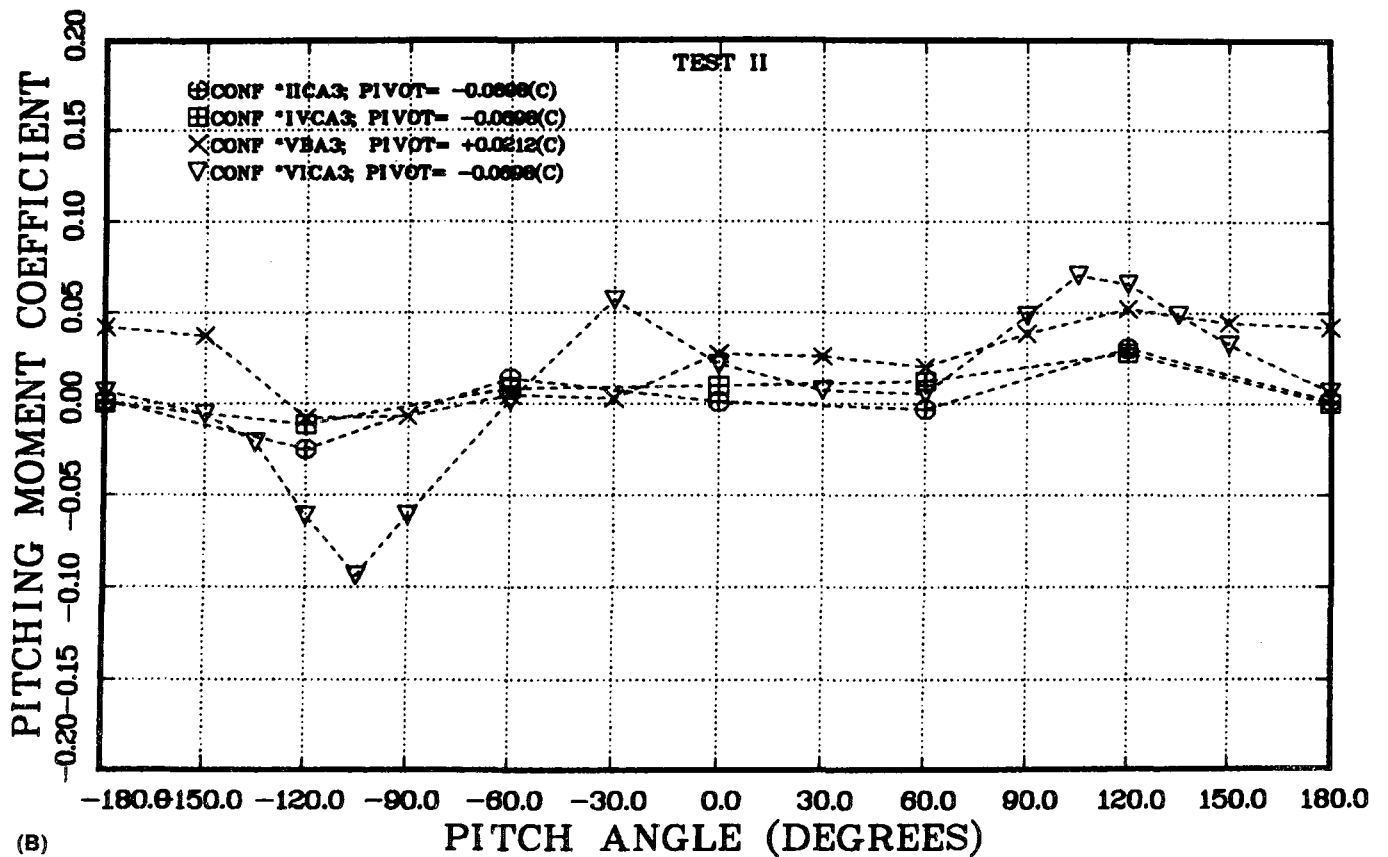
**Figure 14.** The Influence of Upstream Shielding on Collector Pitching Moment Characteristics
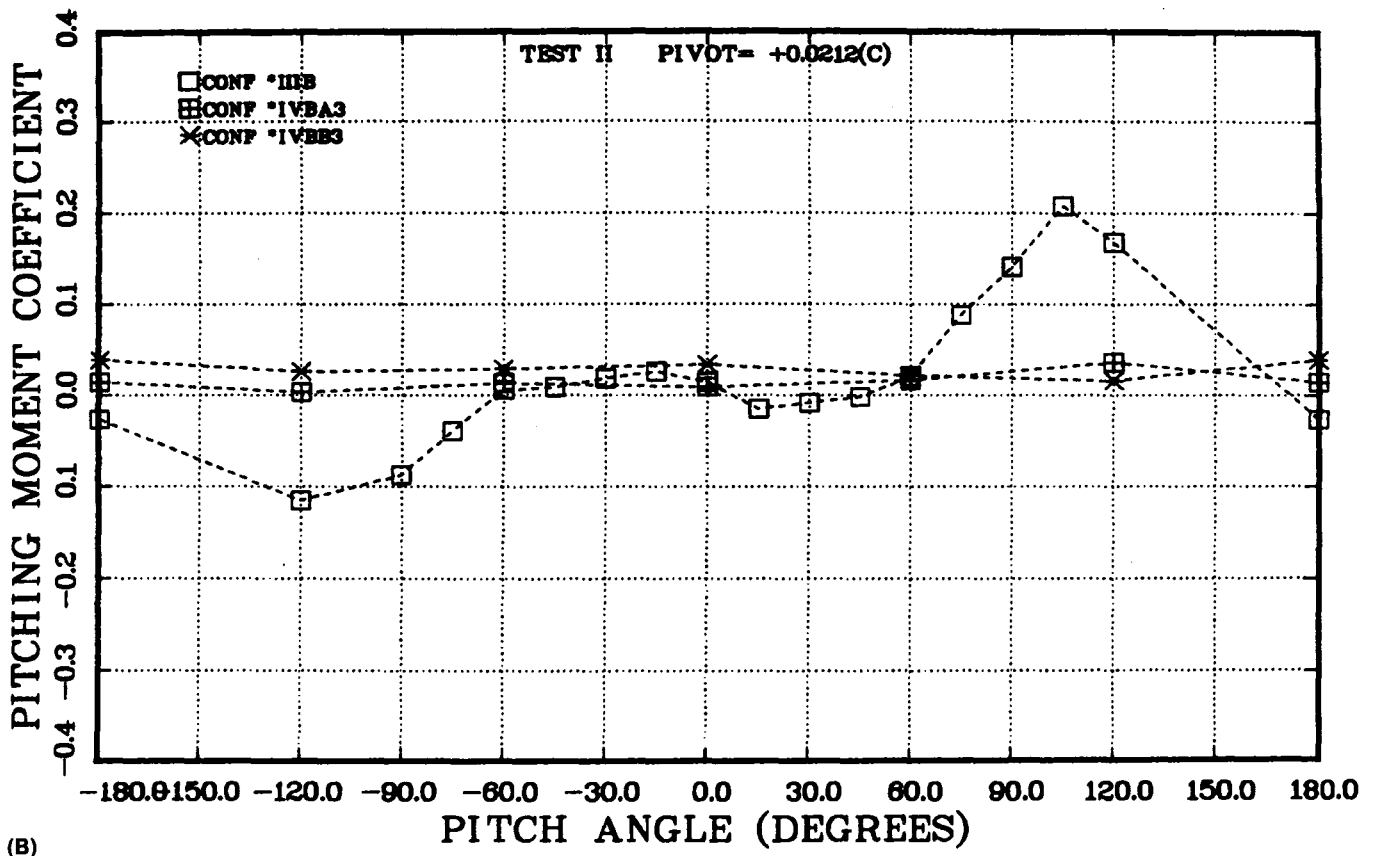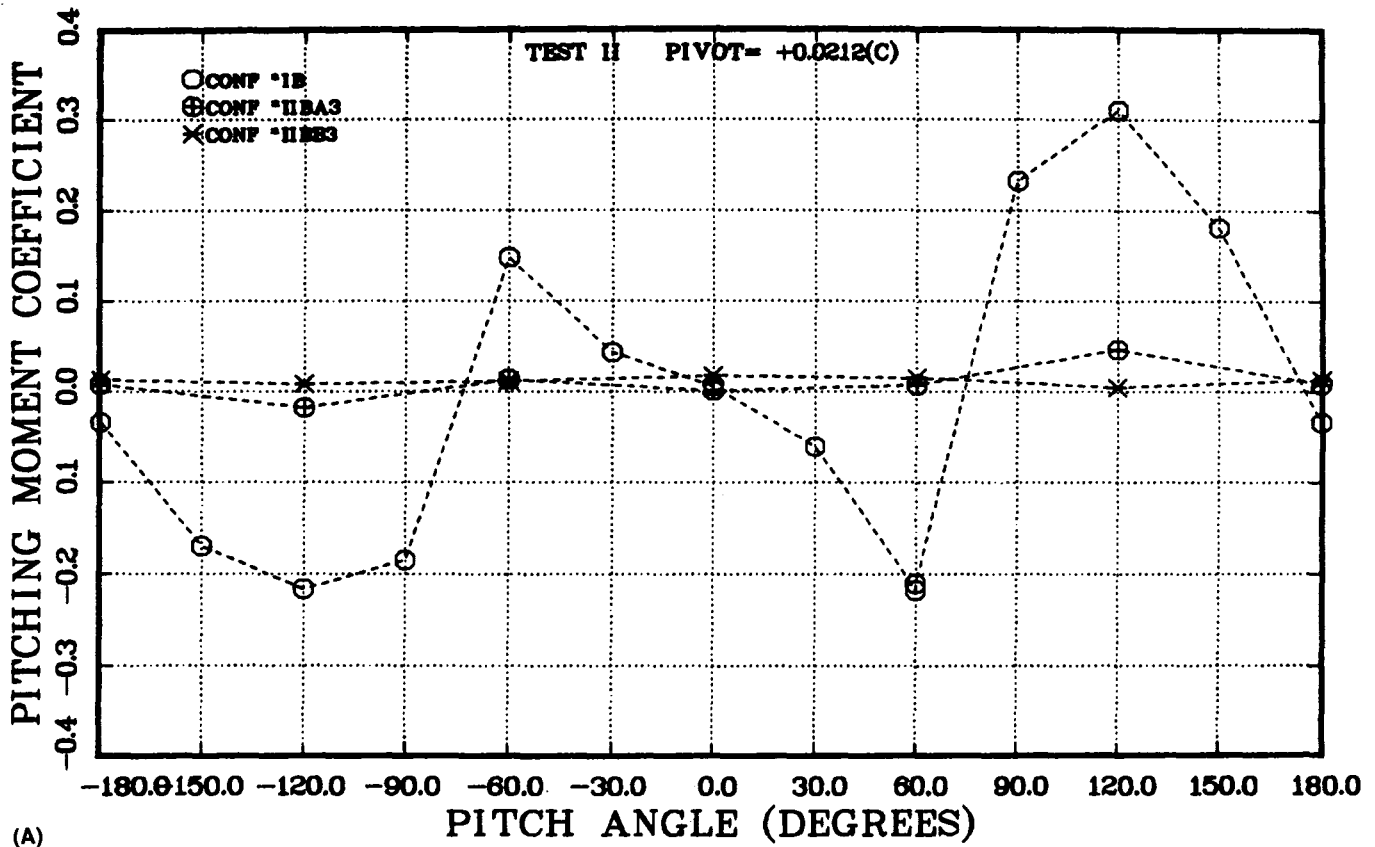
**Figure 15.** Moment Reductions Afforded by Fence Configurations of Varying Porosity for the Intermediate Pivot Location
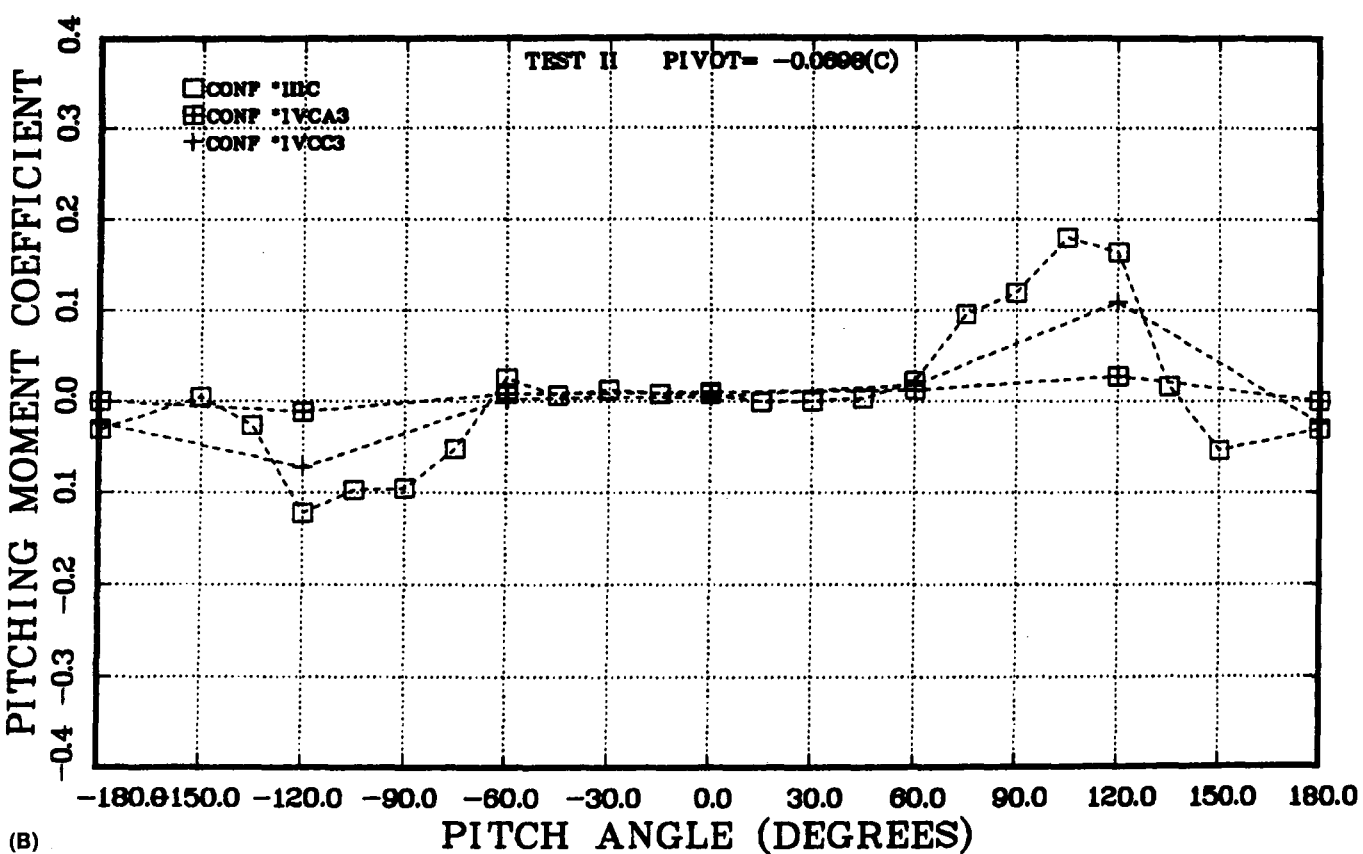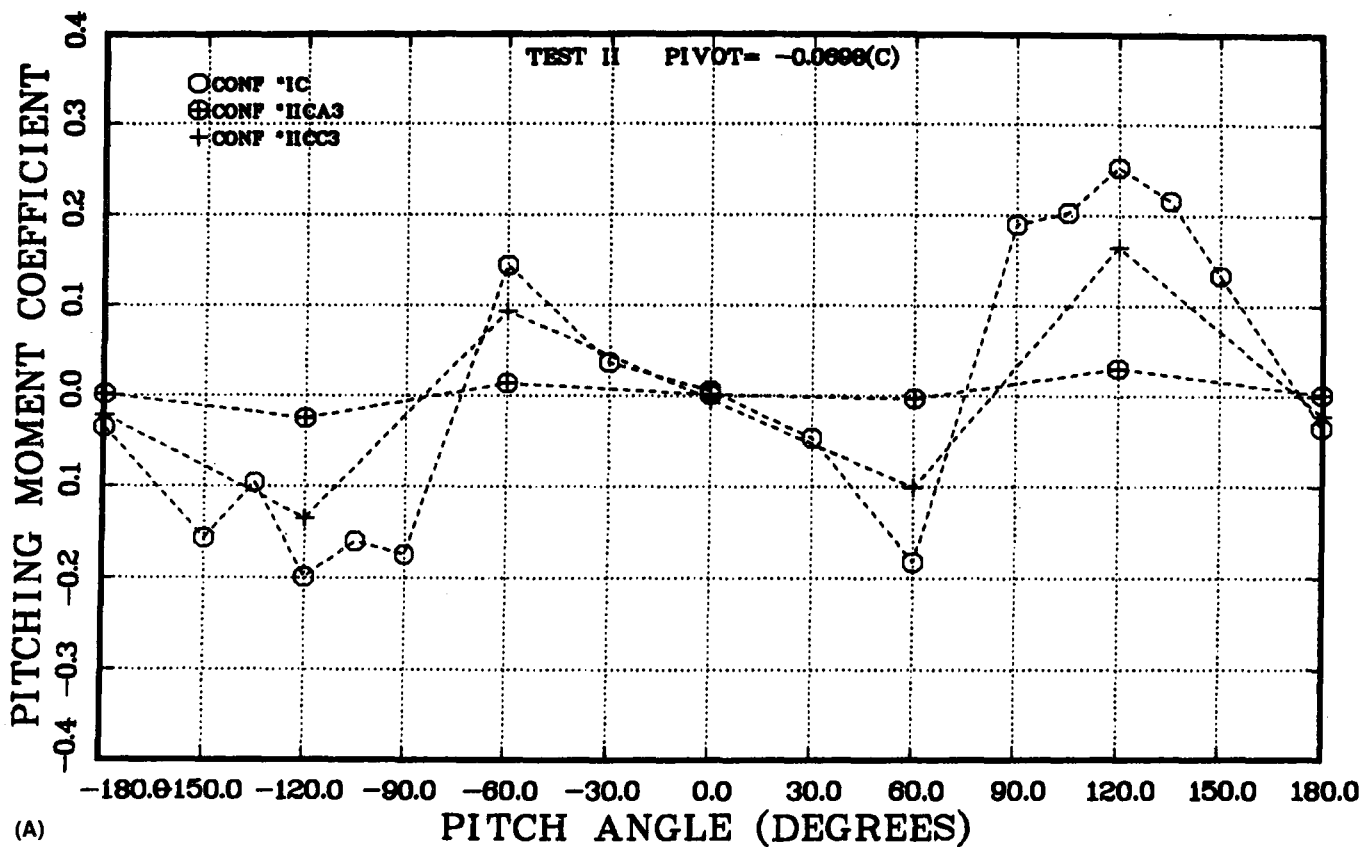
**Figure 16.** Moment Reductions Afforded by Fence Configurations of Varying Porosity for the Forward Pivot Location

## 4.2.4 Fence Spacing Upstream From Perimeter Row

The influence of fence spacing upstream from the perimeter row of an array is illustrated in Figures 17A and 17B for the 40% and 23% porosity fences, respectively. These results indicate that fence spacing upstream from the perimeter row of an array (within the range of 1-1/2 to 5 apertures) exerts no significant influence on the pitching moment characteristics of a perimeter row collector module.
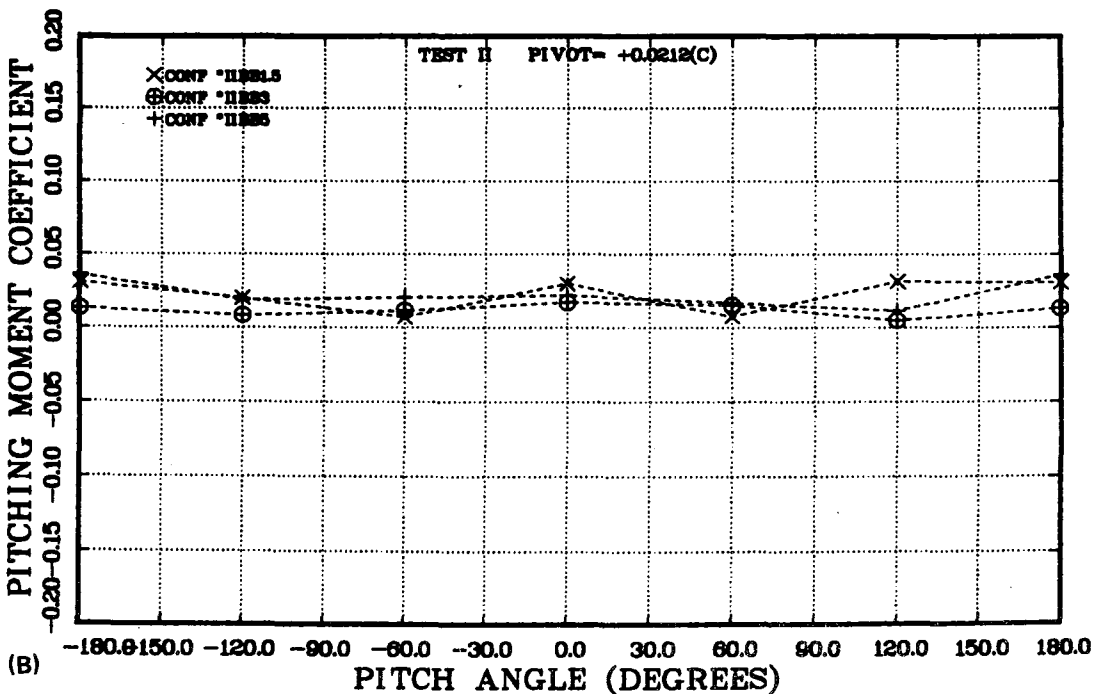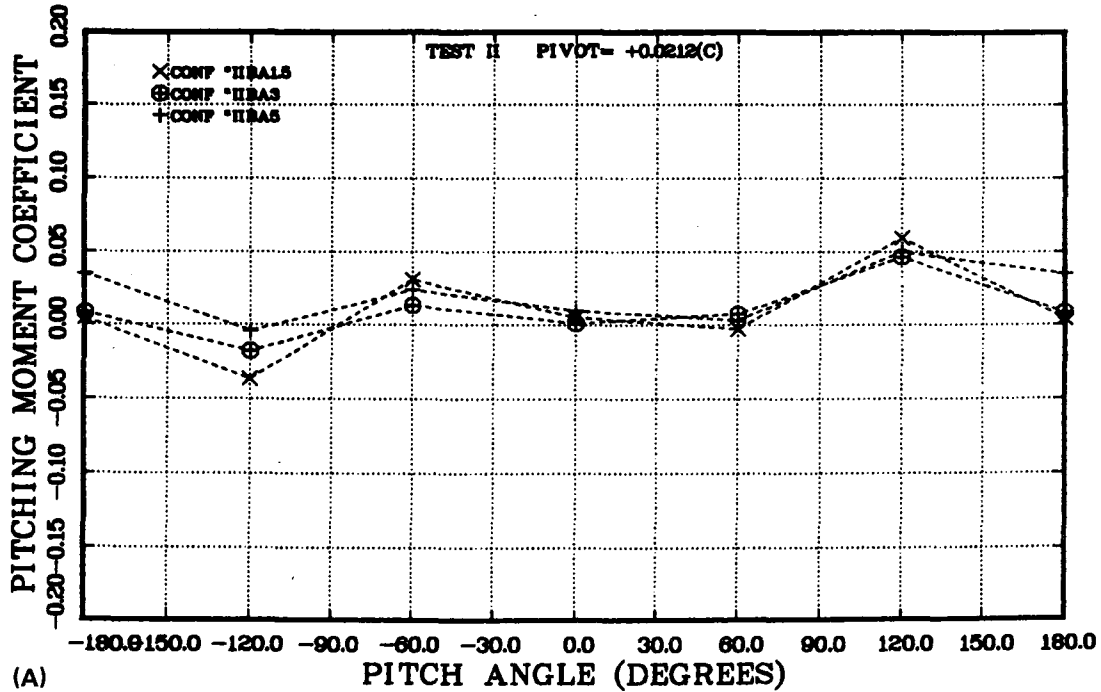


**Figure 17.** The Influence of Fence Spacing Upstream From the Perimeter Row of an Array on Pitching Moment Characteristics

30

## 4.2.5 Fence Porosity

The influence of fence porosity on the pitching-moment characteristics at both the positive and negative peaks is illustrated in Figures 18A and 18B. Data for a perimeter-row module is shown in Figure 18A, while Figure 18B applies to collector modules located in the second row of an array. For all cases, the data indicates that the peak pitching-moment coefficient varies approximately linearly with fence porosity. Furthermore, a fence with a porosity of 50% reduces the peak moment coefficient to approximately one-third the value shown with no fence present.
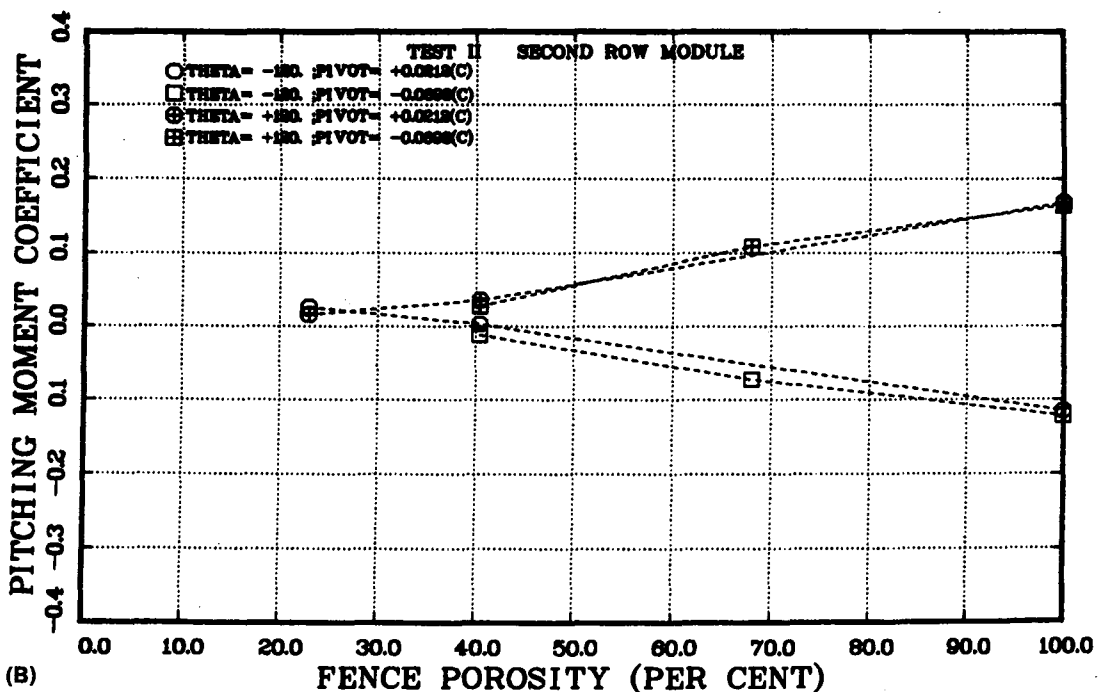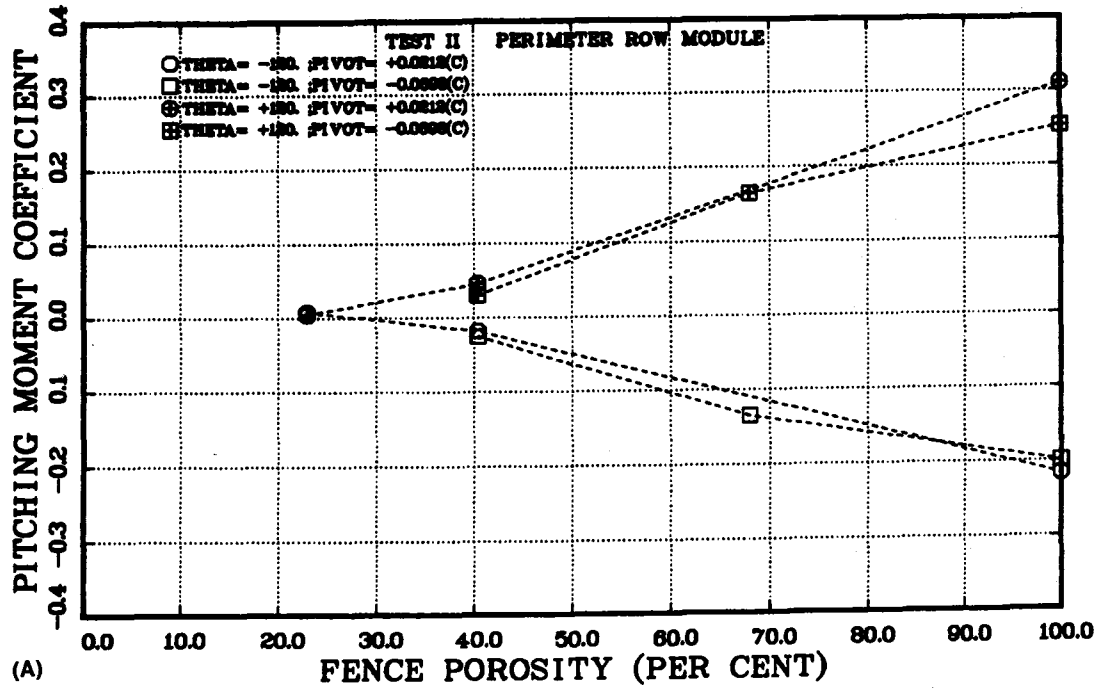


**Figure 18.** The Influence of Fence Porosity on the Pitching Moment Characteristics at Both the Positive and Negative Peaks

# 5. Summary and Conclusions

Two wind-tunnel tests were conducted to define the pitching-moment characteristics of parabolic-trough collector modules. The initial test was conducted in a uniform velocity, low turbulence-flow environment. However, the second test was carried out in a facility providing a partial simulation of the atmospheric boundary-layer flow environment. The influence of flow interference resulting from upstream collector rows within an array and from fences was evaluated. The effect of an alternate pivot-axis location was also investigated.

The following conclusions are drawn from the test results presented:

- Flow interference produced by upstream collector rows of an array or by an appropriate fence results in a significant reduction of the peak pitching-moment coefficients.
- A wind-screen fence with a solidity of 50% or greater reduces the maximum pitching-moment coefficient to one-third of the value experienced by a fully exposed parabolic-trough collector module.
- Fence spacing within the range of 1.5 to 5 apertures upstream from the perimeter row of a collector array has no significant influence on the degree of shielding provided by the fence.
- A shift of the pivot-axis location toward the parabolic-trough center of pressure demonstrated a reduction in the peak pitching-moment coefficient.

## References

[1] J. L. Lindsey, *Force and Pressure Tests of Solar Collector Models in the Vought Corporation Systems Division Low-Speed Wind Tunnel (LSWT 503)*, SAND76-7007 (Albuquerque: Sandia Laboratories, May 1976).

[2] J. A. Peterka, J. M. Sinou, and J. E. Cermak, *Mean Wind Forces on Parabolic-Trough Solar Collectors*, SAND80-7023 (Albuquerque: Sandia National Laboratories, May 1980).

DISTRIBUTION:
DOE/TIC-4500 (Rev 70) UC-62 (215)

AAI Corporation
PO Box 6787
Baltimore, MD 21204

Acurex Aerotherm (2)
485 Clyde Avenue
Mountain View, CA 94042
Attn: J. Vindum
        H. Morse

Advanco Corporation
999 N Sepulveda Blvd
Suite 314
El Segundo, CA 90245

Alpha Solarco (2)
1014 Vine St
Suite 2530
Cincinnati, OH 45202
Attn: D. Carroll
        P. Tykewski

Anaconda Metal Hose Co
698 S Main Street
Waterbury, CT 06720
Attn: W. Genshino

Applied Concepts Corp
PO Box 2760
Reston, VA 22090
Attn: J. S. Hauger

Applied Solar Resources
490 East Pima
Phoenix, AZ 85004
Attn: W. H. Coady

Arizona Public Service Co
Box 21666 MS 1795
Phoenix, AZ 85036
Attn: B. L. Broussard

BDM Corporation
1801 Randolph St
Albuquerque, NM 87106
Attn: T. Reynolds

Battelle Memorial Institute
Pacific Northwest Laboratory
PO Box 999
Richland, WA 99352
Attn: K. Drumheller

Bechtel National, Inc
PO Box 3965
50 Beale St
San Francisco, CA 94119
Attn: E. Y. Lam

Black & Veatch (2)
PO Box 8405
Kansas City, MO 64114
Attn: J. C. Grosskreutz
        D. C. Gray

Bloomer-Fiske, Inc
4000 S Princeton
Chicago, IL 60609
Attn: C. Cain

Budd Co (The)
Fort Washington, PA 19034
Attn: W. W. Dickhart

Budd Co (The)
Plastic R&D Center
356 Executive Drive
Troy, MI 48084
Attn: J. N. Epel

Burns & Roe, Inc
800 Kinderkamack Road
Oradell, NJ 07649
Attn: G. Fontana

Burns & Roe (2)
185 Crossways Park Dr
Woodbury, NY 11797
Attn: R. J. Vodrasket
        J. Wysocki

Carrier Corp
Energy Systems Div
Summit Landing
PO Box 4895
Syracuse, NY 13221
Attn: R. A. English

Corning Glass Co (2)
Corning, NY 14830
Attn: A. F. Shoemaker
        W. Baldwin

DISTRIBUTION (cont):

Custom Engineering, Inc
2805 S Tejon St
Englewood, CO 80110

DSET
Black Canyon Stage
PO Box 185
Phoenix, AZ 85029
Attn: G. A. Zerlaut

Desert Research Inst Energy
Systems Laboratory
1500 Buchanan Blvd
Boulder City, NV 89005
Attn: J. O. Bradley

Donnelly Mirrors, Inc
49 West Third St
Holland, MI 49423
Attn: J. A. Knister

Eaton Corp
Industrial Drives Operations
Cleveland Division
3249 E 80th St
Cleveland, OH 44104
Attn: R. Glatt

Electric Power Research Inst (2)
3412 Hillview Ave
Palo Alto, CA 94303
Attn: J. Cummings
      J. E. Bigger

Energetics
1201 Richardson Dr
Suite 216
Richardson, TX 75080
Attn: G. Bond

Energy Technology Eng Center
PO Box 1449
Canoga Park, CA 91304
Attn: J. Roberts

E-Systems Inc
Energy Tech Center
PO Box 226118
Dallas, TX 75266
Attn: R. R. Walters

Eurodrive, Inc
2001 W Main St
Troy, OH 45373
Attn: S. D. Warner

Exxon Enterprises (3)
PO Box 592
Florham Park, NJ 07923
Attn: J. Hamilton
      P. Joy
      M. C. Noland

Florida Solar Energy Center (2)
300 State Road, Suite 401
Cape Canaveral, FL 32920
Attn: C. Beech
      D. Block

Ford Motor Co
Glass Div, Technical Center
25500 W Outer Drive
Lincoln Park, MI 48246
Attn: V. L. Lindberg

Foster Wheeler Solar Dev Corp
12 Peach Tree Hill Road
Livingston, NJ 07039
Attn: A. C. Gangadharan

General Motors
Harrison Radiator Div
Lockport, NY 14094
Attn: L. Brock

Georgia Power Co (2)
270 Peachtree
PO Box 4545
Atlanta, GA 30302
Attn: J. Roberts
      W. Davis

Glitsch, Inc
PO Box 226227
Dallas, TX 75266
Attn: R. W. McClain

Haveg Industries, Inc
1287 E Imperial Highway
Santa Fe Springs, CA 90670
Attn: J. Flynt

DISTRIBUTION (cont):

Highland Plating
1128 N Highland
Los Angeles, CA 90038
Attn: M. Faeth

Honeywell, Inc
Energy Resources Center
2600 Ridgeway Parkway
Minneapolis, MN 55413
Attn: J. R. Williams

Insights West
900 Wilshire Blvd
Los Angeles, CA 90017
Attn: J. H. Williams

Jacobs Engineering Co
251 S Lake Avenue
Pasadena, CA 91101
Attn: H. Cruse

Jet Propulsion Laboratory (3)
4800 Oak Grove Dr
Pasadena, CA 91103
Attn: J. Becker
      J. Lucas
      V. C. Truscello

Lawrence Livermore Laboratory
University of California
PO Box 808
Livermore, CA 94500
Attn: W. C. Dickinson

Los Alamos National Laboratory
Los Alamos, NM 87545
Attn: C. D. Bankston

McDonnell-Douglas Astronautics Co (3)
5301 Bolsa Ave
Huntington Beach, CA 92647
Attn: J. B. Blackmon
      J. Rogan
      D. Steinmeyer

Meridian Corp (2)
5201 Leesburg Pike, Suite 400
Falls Church, VA 22041
Attn: J. White
      J. Meglen

Morse Chain
Div of Borg-Warner Corp
4650 Steele St
Denver, CO 80211
Attn: G. Fukayama

New Mexico State University
Solar Energy Dept
Las Cruces, NM 88001

Omnium G
1815 Orangethorpe Park
Anaheim, CA 92801
Attn: S. P. Lazzara

Owens-Illinois
1020 N Westwood
Toledo, OH 43614
Attn: Y. K. Pei

PPG Industaries, Inc
One Gateway Center
Pittsburg, PA 15222
Attn: C. R. Frownfelter

Parsons of California
3437 S Airport Way
Stockton, CA 95206
Attn: D. R. Biddle

Schott America
11 E 26th St
New York City, NY 10010
Attn: J. Schrauth

Shelltech Associates
809 Tolman Dr
Stanford, CA 94305
Attn: C. R. Steele

Solar Energy Information Center
1536 Cole Blvd
Golden, CO 80401
Attn: R. Ortiz

Solar Energy Research Inst (6)
1617 Cole Blvd
Golden, CO 80401
Attn: B. L. Butler
      G. Gross
      B. P. Gupta
      F. Kreith
      L. M. Murphy
      J. Thornton

DISTRIBUTION: (cont)

Solar Kinetics, Inc
PO Box 47045
Dallas, TX 75247
Attn: G. Hutchison

Southwest Research Institute
PO Box 28510
San Antonio, TX 78284
Attn: D. M. Deffenbaugh

Stanford Research Institute
Menlo Park, CA 94025
Attn: A. J. Slemmons

Stearns-Roger
4500 Cherry Creek
Denver, CO 80217
Attn: W. R. Lang

W. B. Stine
1230 Grace Dr
Pasadena, CA 91105

Sun Gas Co
Suite 800, 2 N Park E
Dallas, TX 75231
Attn: R. C. Clark

Sundstrand Electric Power
4747 Harrison Ave
Rockford, IL 61101
Attn: A. W. Adam

Sunpower Systems
510 S 52 St
Tempe, AZ 85281
Attn: W. Matlock

Suntec Systems, Inc
2101 Wooddale Dr
St. Paul, MN 55110

Swedlow, Inc (2)
12122 Western Ave
Garden Grove, CA 92645
Attn: E. Nixon
       J. M. Friefeld

TRW, Inc
Energy Systems Group of TRW, Inc
One Space Park, Bldg R4, Rm 2074
Redondo Beach, CA 90278
Attn: J. M. Cherne

Texas Tech University
Dept of Electrical Engineering
PO Box 4709
Lubbock, TX 79409
Attn: J. D. Reichert

3M-Decorative Products Div
209-2N 3M Center
St. Paul, MN 55144
Attn: B. Benson

3M-Product Development
Energy Control Products
207-1W 3M Center
St. Paul, MN 55144
Attn: J. R. Roche

Toltec Industries, Inc
40th and East Main
Clear Lake, IA 50428
Attn: D. Chenault

US Dept of Energy (3)
Albuquerque Operations Office
PO Box 5400
Albuquerque, NM 87185
Attn: G. N. Pappas
       J. A. Morley
       J. Weisiger

US Dept of Energy
Div of Energy Storage Systems
Washington, DC 20585
Attn: J. Gahimer

US Dept of Energy (6)
Div of Solar Thermal Technology
Washington, DC 20585
Attn: G. W. Braun
       J. E. Greyerbiehl
       B. Hochheiser
       C. McFarland
       J. E. Rannels
       F. Wilkins

US Department of Energy
San Francisco Operations Office
1333 Broadway, Wells Fargo Bldg
Oakland, CA 94612
Attn: R. W. Hughey

36

DISTRIBUTION: (cont)

University of New Mexico (2)
Dept of Mechanical Eng
Albuquerque, NM 87113
Attn: M. W. Wilden
      W. A. Cross

Viking
3467 Oceal View Blvd
Glendale, CA 91208
Attn: G. Goranson

Winsmith
Div of UMC Industries, Inc
Springville, NY 14141
Attn: R. Bhise

Wyle Lab
7800 Governor's Dr West
Huntsville, AL 35807
Attn: R. Losey

| | |
|---|---|
| 400 | R. P. Stromberg |
| 1510 | D. B. Hayes |
| 1520 | T. B. Lane |
| 1600 | D. B. Shuster |
| | Attn: D. J. Rigali |
| 1630 | R. C. Maydew |

| | |
|---|---|
| 1634 | D. D. McBride |
| 1634 | D. A. Powers |
| 1634 | R. E. Tate |
| 1652 | D. E. Randall (15) |
| 1810 | R. G. Kepler |
| 1820 | R. E. Whan |
| 1830 | M. J. Davis |
| 1840 | N. J. Magnani |
| 2540 | K. L. Gillespie |
| 3161 | J. E. Mitchell |
| 3600 | R. W. Hunnicutt |
| 3700 | R. R. Russell |
| 8430 | R. C. Wayne |
| 8452 | A. C. Skinrood |
| 8453 | W. R. Delameter |
| 8453 | W. G. Wilson |
| 9000 | G. A. Fowler |
| 9700 | E. H. Beckner |
| 9720 | D. G. Schueler |
| 9721 | J. F. Banas |
| 9722 | J. V. Otts |
| 9725 | R. H. Braasch |
| 9727 | J. A. Leonard |
| 8214 | M. A. Pound |
| 3141 | L. J. Erickson (5) |
| 3151 | W. L. Garner (3) |
| | For DOE/TIC (Unlimited Release) |